AD NUMBER: AD0867427
LIMITATION CHANGES
TO: Approved for public release; distribution is unlimited.
FROM: Further dissemination only as directed by Space and Missile Systems Organization, Norton AFB, CA, 94209.
AUTHORITY
SAMSO ltr dtd 21 Nov 1977

FINAL REPORT
MATERIAL RESPONSE STUDIES (MARS II)
VOLUME II

HIGH HEATING RATE RESPONSE OF TWO MATERIALS FROM 72°F TO 6000°F

by
S. G. Babcock
P. A. Hochstein
L. J. Jacobs

Materials & Structures Laboratory
Manufacturing Development
General Motors Corporation

TECHNICAL REPORT SAMSO TR 69-393, VOL. II
1970, March

Prepared For
Space & Missile Systems Organization
Deputy for Ballistic Missile Re-entry Systems
Air Force Systems Command
Norton Air Force Base, California 92409
Contract No. F04701-68-C-0161

FINAL REPORT
MATERIAL RESPONSE STUDIES (MARS II)
VOLUME II

HIGH HEATING RATE RESPONSE OF TWO MATERIALS FROM 72°F TO 6000°F

by
S. G. Babcock
P. A. Hochstein
L. J. Jacobs

Materials & Structures Laboratory
Manufacturing Development
General Motors Corporation

FOREWORD

This report was prepared by the Applied Mechanics Section of the Materials and Structures Laboratory, Manufacturing Development, General Motors Corporation, General Motors Technical Center, Warren, Michigan, under Air Force Contract F04701-68-C-0161. The work was performed during the period 1 April 1968 to 31 August 1969 and was administered by the Air Force and Missile Systems Organization, Air Force System Command, with Major N. J. Azzarita and Lt. T. Graham as the technical administrators. Mr. R. B. Mortensen, Mr. J. G. Koehler, Mr. R. A. Needham, Dr. F. A. Field, Mr. W. F. Davenport and Dr. R. M. Jones of the Aerospace Corporation served as principal technical monitors for the Air Force.

Because of the different types of work performed under this program, Material Response Studies II, the report is divided into two separately bound volumes. The first volume is entitled "Multiaxial Loading Behavior of Four Materials Including ATJ-S Graphite and RAD-6300 Carbon Phenolic", and the second volume is entitled "High Heating Rate Response of Two Materials from 72 to 6000°F".

The work was performed under the supervision of Mr. S. J. Green. Program manager and principal investigator was Mr. S. G. Babcock. Other project scientists included Mr. R. D. Perkins, Mr. J. D. Leasia, Mr. F. L. Schierloh, Mr. P. A. Hochstein, Mr. L. J. Jacobs, and Dr. A. H. Jones.

The authors would like to thank Messrs. M. C. Klewicki and L. A. Seltz for their efficient technical assistance in obtaining the experimental data on the biaxial strain rate equipment, and Mr. R. D. Chaney and Mrs. W. I. Trippen for their help in reducing the data. Acknowledgements are given to Mr. G. T. Harkins and Mr. J. George for their assistance in designing and building the high heating rate machine, and Mr. G. Hopewell and Mr. J. A. Bonner for conducting the tests, and especially to Dr. C. J. Maiden for his support of the program.

This report is UNCLASSIFIED. This document may be further distributed by any holder only with specific prior approval of Space and Missile Systems Organization (SMYSE), Norton AFB, California 92409.

This technical report has been reviewed and is approved.

Robert J. Might
Lieutenant, USAF
Project Officer
SAMSO/SMYSE

ABSTRACT

This report describes the results of a study to characterize two graphitic materials, graphite (ATJ-S) and carbon phenolic (RAD 6300), in uniaxial stress after undergoing heating to temperature near 6500°F. Heating rates up to 1000°F/second and strain rates up to 10/second were investigated. Test results as well as a complete description of the experimental techniques developed in this program are discussed. Techniques include measuring strain using a laser extensometer, coating thin films on graphite using r.f. sputtering, and determining true test temperature.

TABLE OF CONTENTS

LIST OF ILLUSTRATIONS

LIST OF ILLUSTRATIONS (Continued)

LIST OF ILLUSTRATIONS
IN APPENDIX

LIST OF TABLES

(page viii is blank)

INTRODUCTION

The potential severe environment reentry vehicles may encounter, including very short time and high temperature loadings, predicates the need for engineering material properties under similar conditions. These conditions include high heating rates up to temperatures near sublimation followed by mechanical loading at high strain rate.

This program started as MARS I,[1] where various heating techniques were investigated to characterize typical R/V materials. It was noted that early investigators[2-7] suffered from limitations that either prevented heating the materials under study rapidly or performing short time loading after heating. Analytical techniques were also developed in MARS I to predict the temperature profile and thermal stress profile of an ablating cylindrical specimen subjected to a heat source either at the surface or in-depth. It was shown that very high thermal stresses can be introduced where surface heating techniques are involved. Experimental investigations were conducted on surface techniques such as plasma arc and arc image heating. In-depth techniques studied were direct resistance, induction, dielectric, and electron beam heating. Advantages and disadvantages for each technique were discussed along with general difficulties encountered in testing at very high temperature such as temperature measurement.

As a result of the MARS I study, a direct resistance heating technique was chosen because of relative ease of adaption to the present strain rate equipment at General Motors. Section I discusses the design considerations in the new technique.

In addition, a unique system to measure strain on test samples at temperatures up to 6500°F is described. This laser extensometer is able to track gage marks coated onto graphitic materials by an r.f. sputtering technique. The design philosophy behind r.f. sputtering is discussed as well as philosophy of measuring temperature near graphite sublimation.

Section II describes the test results on two materials: graphite (ATJ-S) and carbon phenolic (RAD 6300). In addition, a study to determine the "explosion threshold" of carbon phenolic is described where an upper limit on heating rate was determined above which the test material literally blows apart. Section III reviews the conclusions drawn from the entire MARS II investigation on high temperature properties of materials. An Appendix is included in order to correlate test results from several investigations on RAD 6300 carbon phenolic up to temperatures of 800°F.

SECTION I
DESCRIPTION OF TEST TECHNIQUE

STRAIN RATE MACHINE

The technique developed in this program was designed to test electrically conductive materials in uniaxial tension or compression at constant strain rates. Prior to deformation, the test sample can be "in-depth" heated at constant heating rates up to temperatures in excess of 6000°F. After achieving a designated test temperature, testing can be initiated immediately or after a given hold time. Thus heating rate and/or time-at-temperature studies can be conducted.

To achieve constant strain rate tests at rates of 10^{-3} to about 10^{2}/second, a gas-operated driving piston (Figure 1) moves according to the rate of gas discharge from one side of the piston or the other. Orifice plate diameter, gas pressure, viscous damper setting, and specimen resistance combine to ultimately determine the exact rate of loading for a particular test.[8] Inertia effects are negligible up to rates near 30-50/second, depending on the material being tested.

For a typical test, temperature during heat up is recorded on a strip chart recorder while load and displacement during the mechanical deformation are recorded on Polaroid film taken from a dual beam cathode ray oscilloscope. Scope triggering is initiated through a shorting wire located in the gas discharge line on the loading cylinder. This extremely

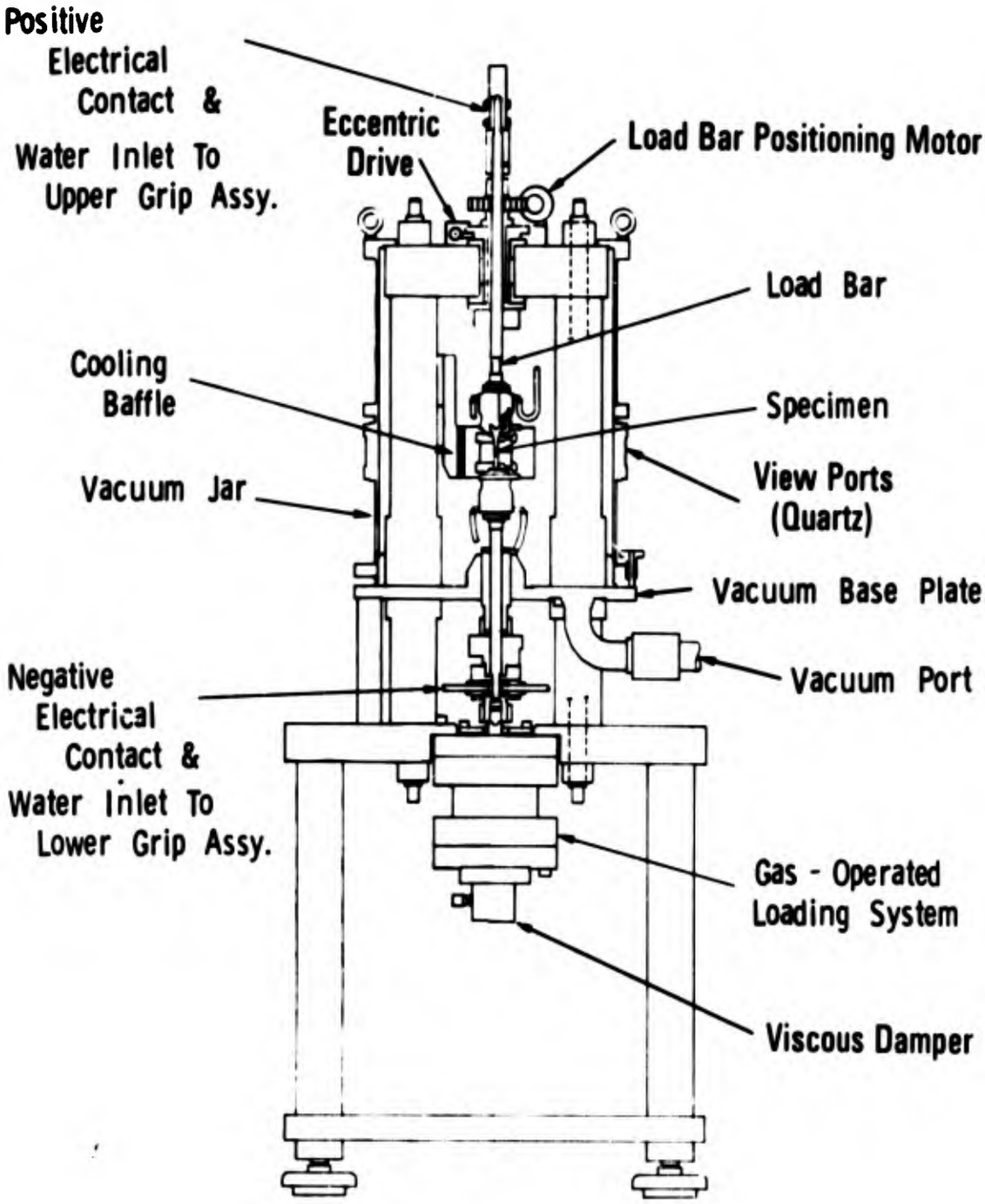

Figure 1 Schematic of High Temperature Medium Strain Rate Machine

sensitive technique senses the first motion of gas upon rapid opening of the discharge valve. Data reduction techniques are discussed in Reference 8. Figures 2 and 3 are photographs of the complete test setup.

Load is measured from semiconductor strain gages mounted on the water-cooled elastic load bar directly above the specimen. This load bar is completely removable and can be calibrated statically with standard load cells. An AC carrier plug-in strain gage monitor is used with the dual beam oscilloscope. Through an electronic switching panel, either uniaxial load or bending load in two orthogonal directions can be measured. Specimen pretest alignment is obtained by eliminating bending at the strain gage location on the load bar. This is accomplished by rotation of two concentric offset plates (Figure 1) onto which the load bar rests during a test. The upper end of the load bar can move horizontally up to 0.005 inch, which is sufficient to eliminate bending in closely toleranced specimens. Calibration tests have been conducted to verify that when bending is eliminated in the load bar, bending is also eliminated in the test specimen. An automatic servo-controlled hydraulic cylinder in series with the upper load bar maintains a preset load applied to a test specimen prior to testing in order to minimize any softness or slack in the grip assembly. It was necessary to design an automatic preload system in order to maintain a constant load while heating materials that thermally expand (or contract) large amounts at high heating rates.

Basically, the servo system (Figure 4) consists of a double-acting hydraulic "pancake" cylinder in "series" with the load bar. The cylinder is operated by means of a fast, proportional, hydraulic servo valve. The servo valve receives an

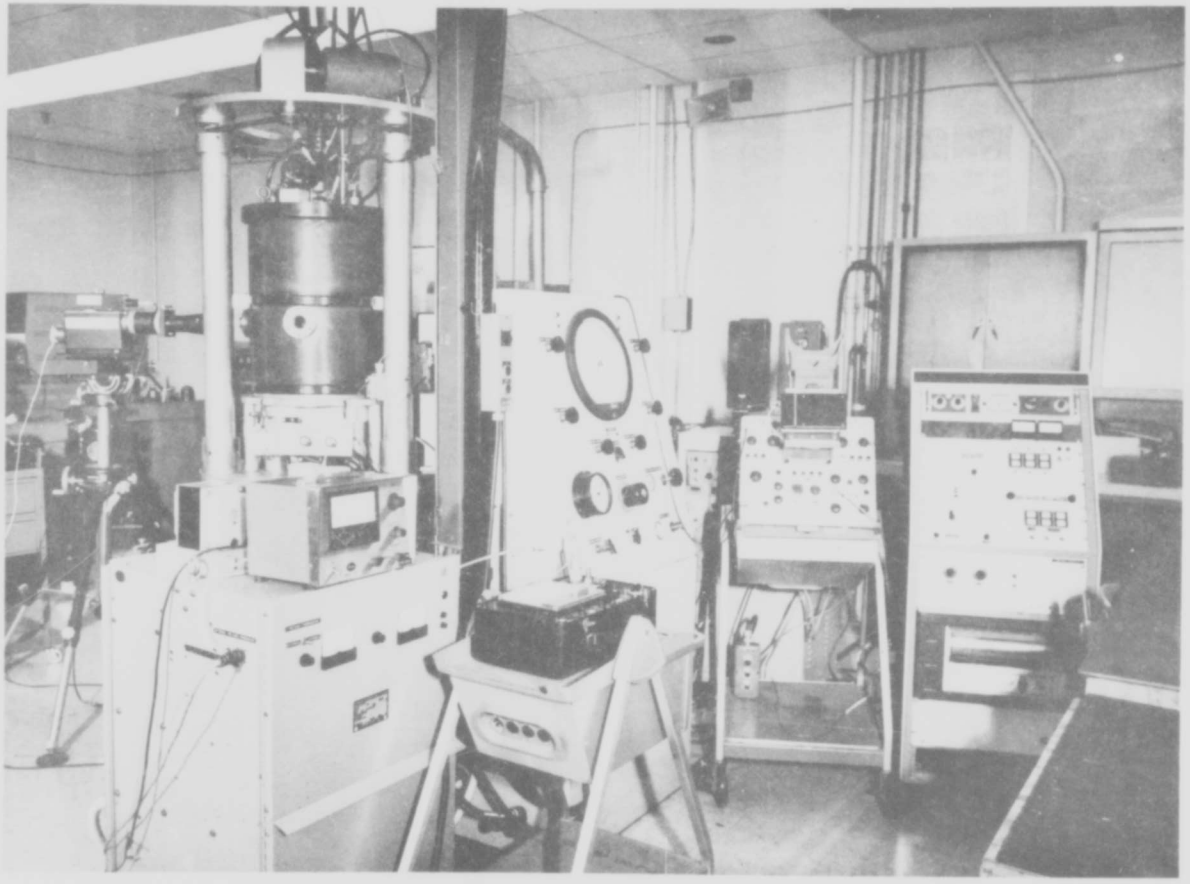

Figure 2 Photograph of High Temperature Testing Facility

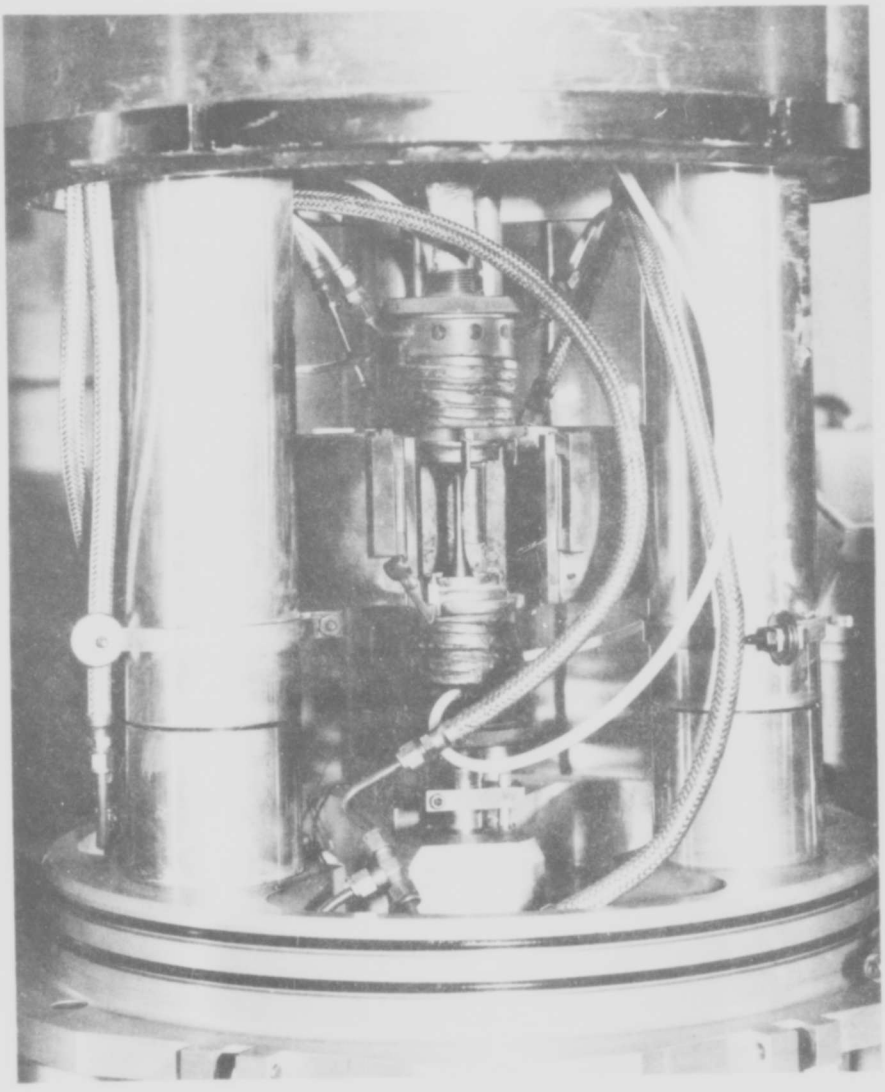

Figure 3 Closeup Photograph of Specimen - Grip Area

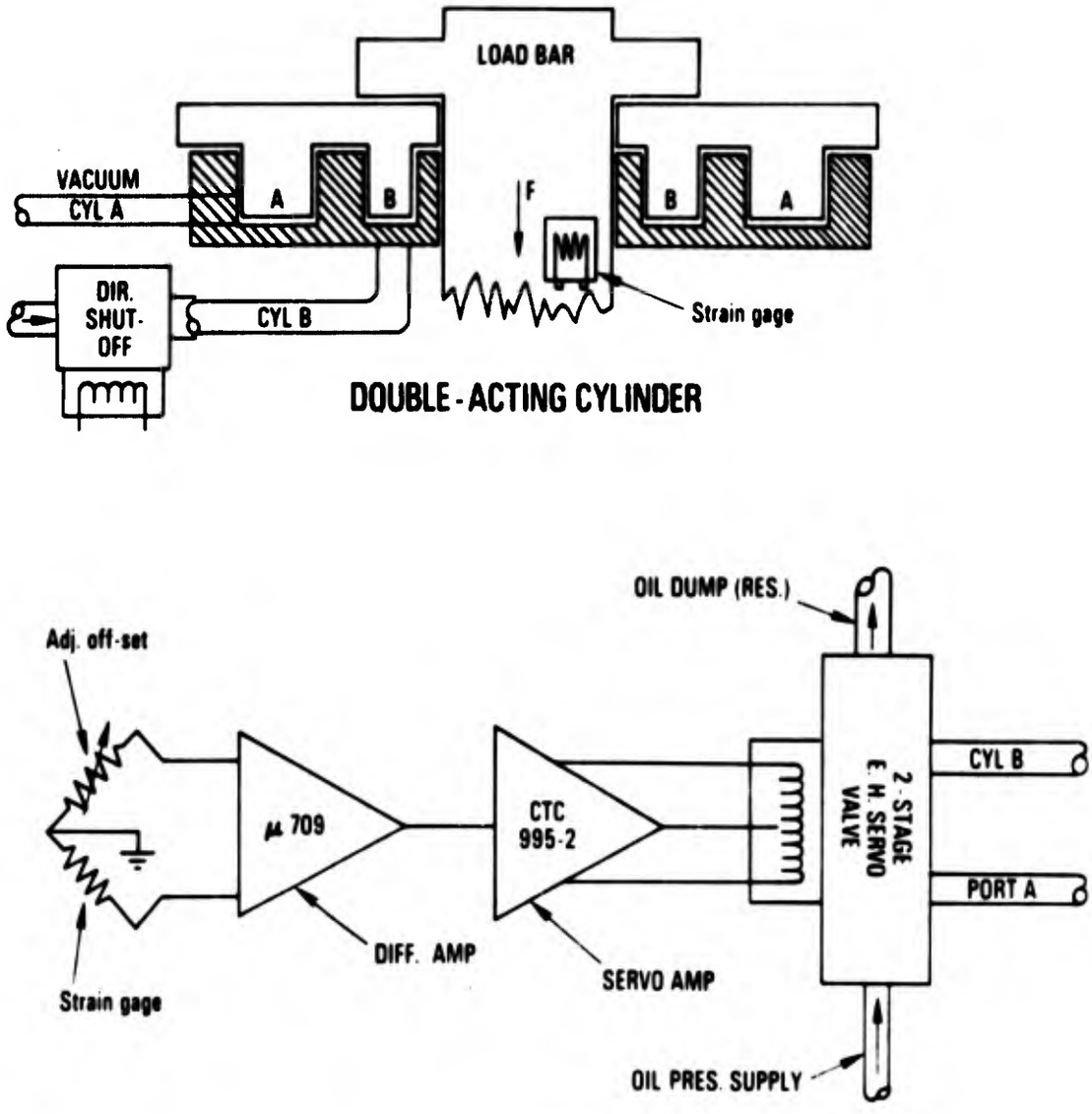

Figure 4 Schematic of Electro-Hydraulic Servo Proportioning System

error signal from a servo amplifier whose differential input determines the magnitude of output error signal. One input to the differential amplifier is controlled by strain gages on the load bar, while the other input is a variable set-point potentiometer, allowing any degree of offset, and hence preload, to be achieved. Servo-control elements are closely coupled to optimize system response time (typically 30 H_z). A high pressure cylinder isolation valve precludes oil seepage during the actual testing period.

The heating of electrically conductive materials is accomplished through a direct resistance method. An 800 ampere, 50 volt regulated direct current power supply, capable of 1200 ampere outputs for periods up to one second, is connected to the test sample through copper electrodes. Specimen grip design allows temperature extremes of 6500 to 7000°F on graphite materials while maintaining moderate temperatures (below 1500°F) in the grip jaws and load bars. In order to achieve temperatures above 5000°F, specimen radiation losses have to be minimized. This is accomplished by surrounding the specimen-grip area with a cast alumina and boron nitride shield into which a graphite felt and pyrolytic graphite liner is placed. Two small holes accommodate material outgassing and optical viewing of the specimen. A freon-cooled baffle surrounds the radiation shield and condenses vapors emanating from the hot samples. This prevents contaminating the vacuum pumping system, which will maintain a specimen environmental pressure as low as one micron of mercury.

In order to achieve precise and repeatable heating profiles from test to test, the power supply is coupled to a high speed temperature controller and predetermined heating rates and time-at-temperature can be programmed.

STRAIN MEASURING TECHNIQUE

Measuring strain on tensile samples is difficult primarily due to the non-uniform gauge section on the specimen. Conventional techniques such as using strain gages or mechanical extensometers suffer drawbacks when used at high temperature or high loading rates. Even the most sophisticated commercially available optical tracking systems are inadequate at temperatures where gauge marks will not adhere to the sample or radiant glow from the specimen interferes with the tracker response. To circumvent these problems, an optical strain measuring technique was designed that will measure small dynamic strains on samples of materials at temperatures up to graphite sublimation.

In conventional optical tracking systems, an optical image of the specimen surface is focused upon a vidicon-type photo tube, wherein a finely focused scanning electron beam sequentially addresses the photo cathode. Previously located "demarcation lines" on the specimen surface--i.e., a well defined area on the specimen with contrasting light and dark areas, serve as the gage section (Figure 5). Any increase in length of this gage section can be detected by the scanning electron beam as a change in "time of intercept" of the fixed frequency scanning voltage. This time domain information is subsequently processed and displayed. Typically, black and white pigment organic based paints are useful to approximately 800°F. Above these temperatures some other form of coating must be used. Small integral steps or tabs on the tensile specimen body could be used but for the local stress concentrations and high temperature gradients which result. Monitoring end-point or grip motion is undesirable at low

ROOM TEMPERATURE TENSILE SPECIMENS

HIGH TEMPERATURE TENSILE SPECIMEN WITH REFRACTORY GAGE BANDS

Figure 5 Photographs of Test Specimens

strain levels because of the complex specimen geometry and inherent gripping problems.

Assuming that the problem of defining a given reference gage section on the test sample at elevated temperatures could be solved, the conventional optical tracking instruments would only prove usable to temperatures at which the blackbody radiation from the specimen did not interfere with the strain measurement. Since the spectral bandwidth of conventional optical extensometers (or trackers) is rather wide, the optical interaction limit generally restricts their use to specimen temperatures below 2000°F. While selective filtering might be used, the already marginal luminous sensitivity of these devices imposes further problems.

In view of the above difficulties in modifying existing instrumentation to measure dynamic strains on specimens at temperatures in excess of 6500°F, new techniques and concepts were examined. From a cursory examination of the blackbody radiation curves for materials at elevated temperatures, it is obvious that if optical interference is to be eliminated in a measuring device, then the band pass of the instrument must lie above the short wave length cut-off for a given temperature (Figure 6). The blackbody noise contributed by the hot specimen can further be reduced by decreasing the optical bandwidth of the measuring instrument. For the instrument design in this study, the actual operating wavelength was chosen with the above criteria in mind. Additionally, the availability of an argon ion laser with significant energy output in the region of interest helped establish the operating spectrum.

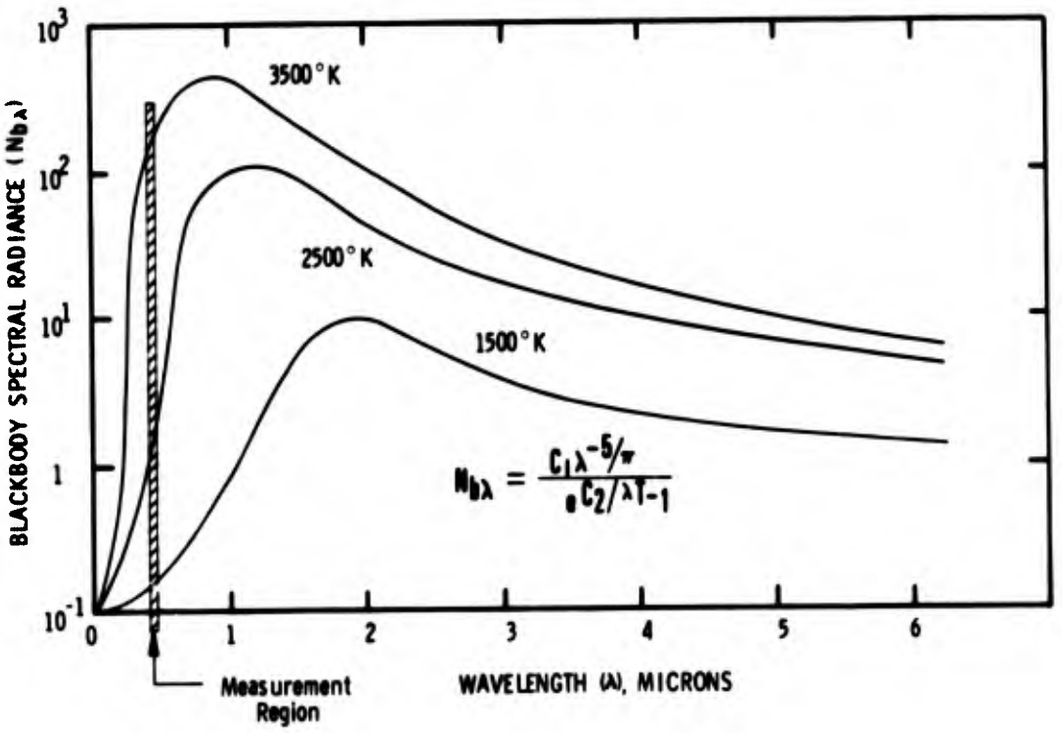

Figure 6 Typical Plank Blackbody Spectral Distributions with Operating Bandpass of Scanning Laser Extensometer

In essence the new strain measuring device, or laser extensometer described herein, operates in almost a reverse mode compared to conventional instruments of like function. Instead of "disecting" an image of the gage section with a scanning electron beam, we chose to scan the illuminating light beam and monitor the returned image with photomultiplier detectors. A brief explanation of the system follows: (Figure 7)

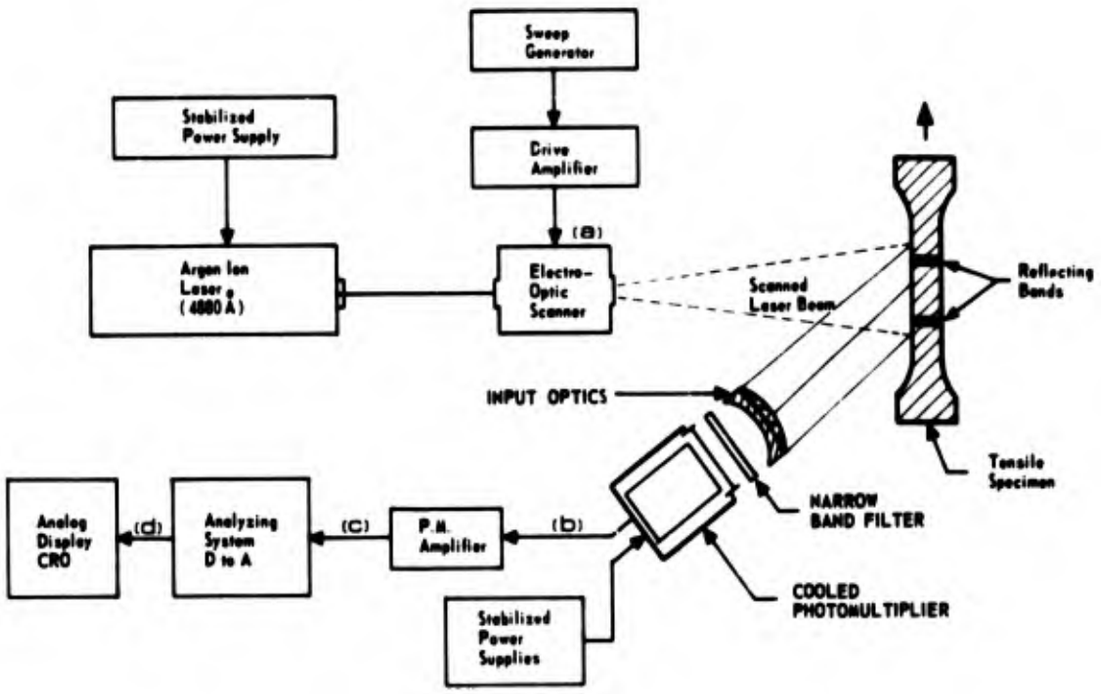

Figure 7 Pictorial Operating Schematic of Laser Extensometer System

1. The laser beam is scanned by an optical element to illuminate the gage section of the tensile test specimen.

2. The reflected light is focused by a lens system through a narrow-band laser spike filter onto a photomultiplier tube.

3. The electrical output signal from the photo-tube is analyzed.

An inherent advantage of scanning the light source rather than the gage section image is that with a fixed (source) beam power density, all the energy reflected from the specimen at any given instant in time may be used to generate a data point. If, however, the entire gage section of the specimen were illuminated, the average power density at the sample surface would be significantly lower; while image analysis would still proceed on a point by point basis.

Light Source and Optics

In actual practice, an argon ion laser is operated single mode at 4880 Å. A nominal beam diameter of 0.5 mm is utilized with an average power of 10 mw, yielding a beam power density of about 5×10^{-2} w/mm^2. This power density was deemed necessary since at 6750°F (4000°K) the power density at the specimen surface (if emissivity is 1) is nominally 10 w/mm^2. It can be shown[1] that for a blackbody at 4000°K, the energy falling within a bandwidth of 10 Å at 4880 Å is equal to approximately 8×10^{-6} w/mm^2. Therefore, to maximize the signal-to-noise (optical) ratio of the system, a very narrow bank interference filter tuned to the laser operating wavelength of 4880 Å is used. While actually less than half the radiation emanating from the luminous specimen is collected by the input optics of the instrument, only about 1% of the laser beam energy is reflected by the surface of the sample. Therefore, only 5×10^{-4} w/mm^2 of 4880 Å radiation is to be detected in $\sim 4 \times 10^{-6}$ w/mm^2 of background noise. The latter figures hold the key to the ultimate success or failure of the device, since an insufficient signal-to-noise ratio would have swamped

the return signal in specimen-generated optical noise. Actual experimental tests on 6000°F (3600°K) specimens yielded signal-to-noise ratios of 70:1.

As is seen in Figure 8, the maximum spatial resolution of the extensometer is limited by the random jitter (noise) in the received signal. This jitter is due to thermal noise in the phototube, a less than ideal spot size in the scanning beam, and optical degradation of the gage section.

Gage Section

If the coating used to generate a gage section on a test sample has a vastly different emissivity than the substrate, then a temperature gradient in the specimen is expected. To alleviate the problem, only two small bands of material were coated onto the tensile specimen so as not to change the critical temperature distribution.

The task of applying adherent coatings to high temperature tensile test specimens became fairly involved. Firstly, very few coatings are stable at temperatures in excess of 6500°F, and secondly, the reflectivity of the coated area has to remain different than that of the underlying substrate in order for the scanning laser beam to be able to detect the boundary of the gage section. Obviously no organic coatings (other than organo-metallics such as tungsten carbonyl) could be considered. Therefore, methods of applying thin films of refractory metals were examined in detail. Since most of the testing was to be conducted on graphitic materials, a metallic or ceramic coating which would form a stable carbide at very high temperatures was considered. The vapor pressures of non-carbide forming noble metals obviated their use. Both tantalum and

hafnium (singly and in combination) form carbides (Hf_2C and Ta_2C) and a compound carbide which has the highest melting point of any known material. Hafnium-tantalum carbides are typically stable to temperatures in excess of 7000°F. These carbides also exist over a relatively large range of stoichiometries.

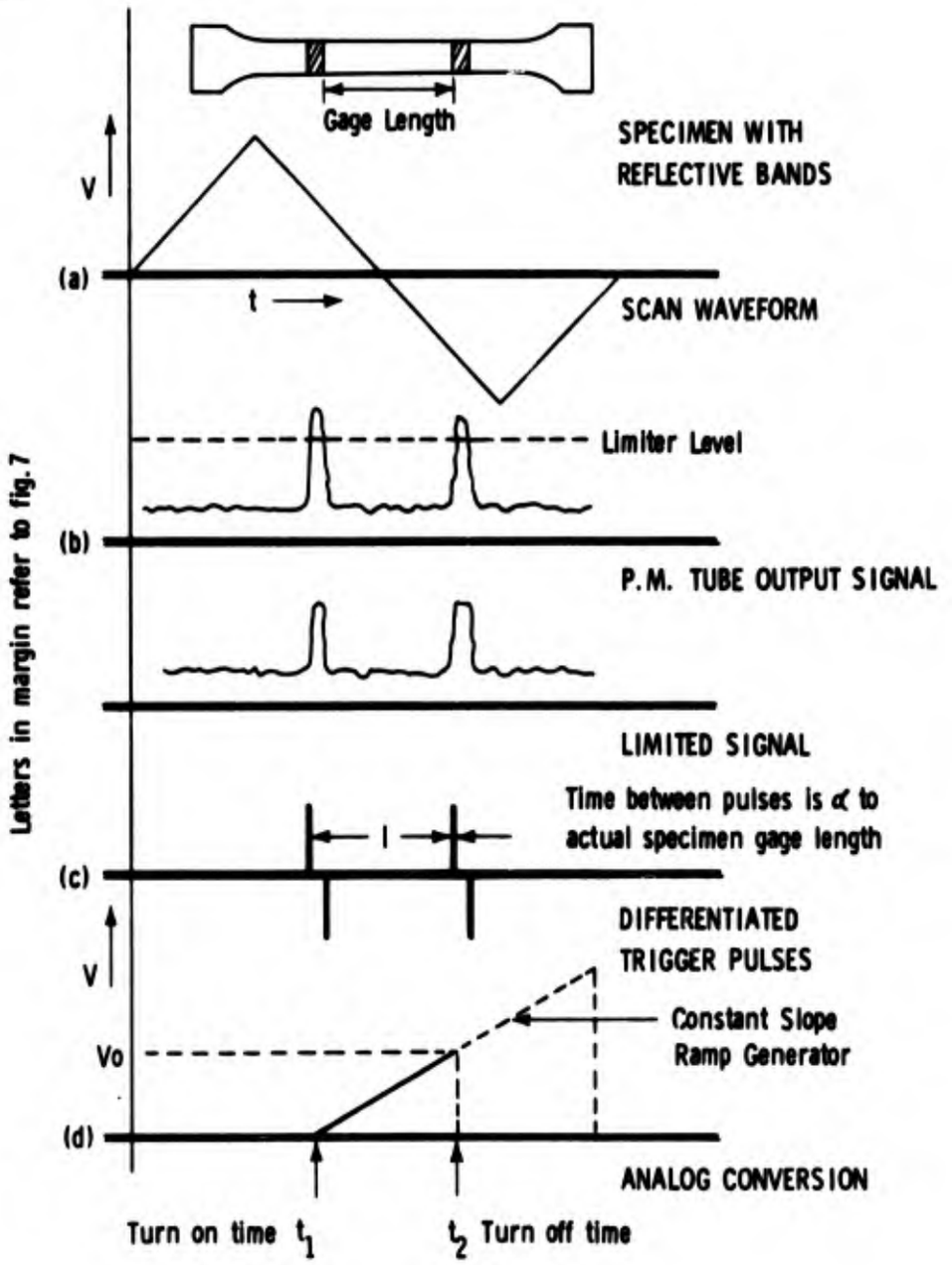

Figure 8 Typical Scan Waveforms & Intercept Signals From a Tensile Specimen

Initial attempts at depositing thin films of both tantalum and hafnium onto graphite substrates did not prove to be successful, as these films flaked off during heating. Adhesion at room temperature was not particularly satisfactory either. Radio frequency sputtering seemed to offer interesting possibilities, so an investigative program was initiated; several grades of "pure" graphite including ATJ-S were chemically cleaned in vacua in excess of 10^{-6} mm Hg for several hours.

Subsequent r.f. etching removed any remaining surface contaminants. Without breaking vacuum, 5-10 micron thick films of both hafnium (99.99%) and tantalum (99.999%) were deposited onto the graphite substrates through a mask which provided a sharp edge definition.

When the samples were later heated in vacuum and in argon, the thin films reacted with the substrate forming the necessary carbide. The carbide formation temperatures were typically below 1200°F for relatively long heating times (> 15 sec). A summary of the measured spectral emissivities of the specimens which were coated are included in Figure 9.

Since emissivity is generally defined as the reciprocal of reflectivity, the relative emissivity values derived for the coated graphite specimens may be translated into spectral reflectivities. Emissivity measurements were made with a spectroradiometer and an automatic micro-optical pyrometer operating at 6000 Å. Computer generated National Bureau of Standards emissivity correction tables were then applied to the data.

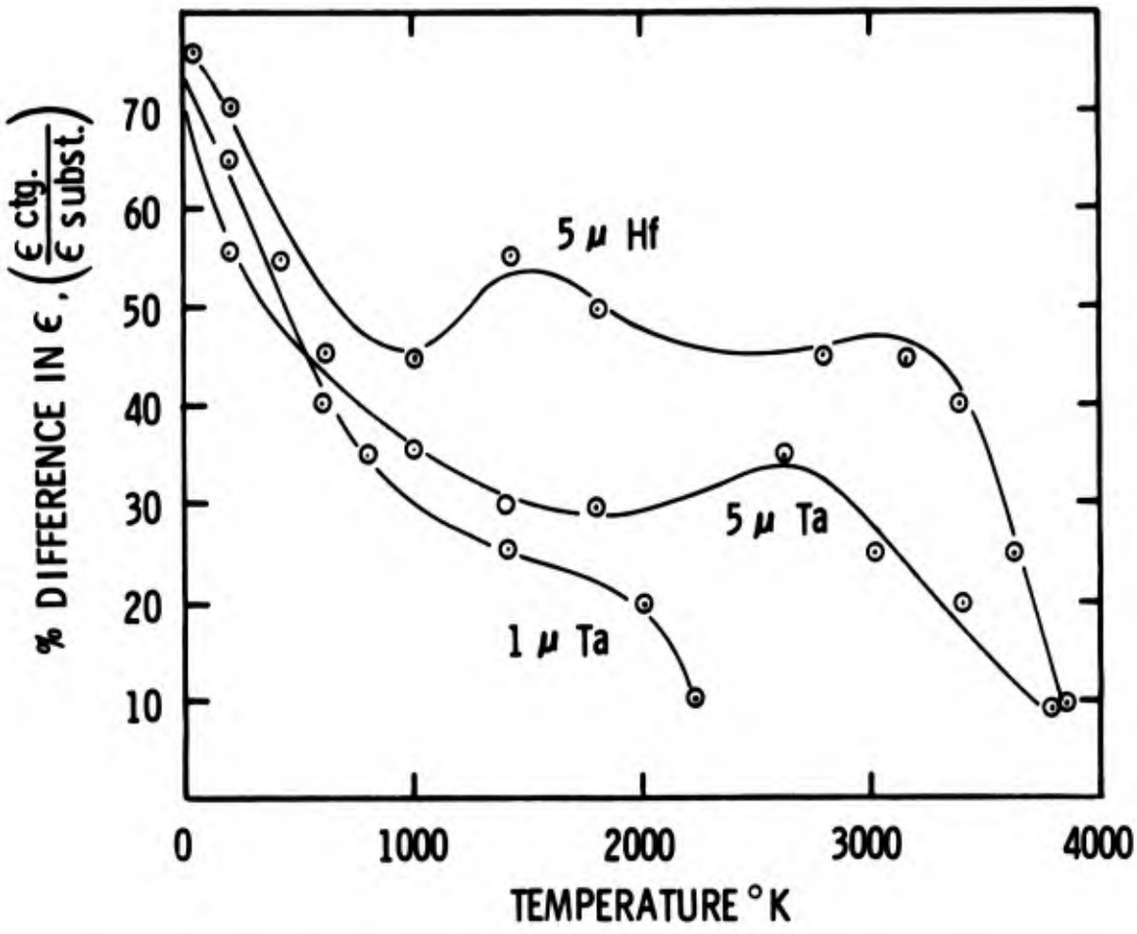

Figure 9 Effective Spectral Emittance (4880 Å) of Thin Film Sputtered Coatings on ATJ-S Graphite

Direct spectral reflectivity measurements were not made with the argon laser since it was not available until a much later date. Preliminary comparisons between the emissivity derived data and that recently run with the argon laser shows a fairly reasonable correlation (± 15%).

It may be worthwhile mentioning that films thinner than 5 μ were evidently transparent and showed little tendencies to assume emissivities vastly different than those of the substrates.

Accuracy and Resolution

Initial design parameters required that the strain measuring device be capable of resolving 10^2 data points per strain rate test, the shortest of which would be of 10^{-3} sec duration. Since the scanning laser beam generates one data point per scan, a scan period of 10^{-5} sec is required. Dynamically scanning a light beam at a 100 KHz rate is not a particularly easy task, since the linearity requirements are fairly stringent. Minimal detectable strain levels of 1% were to be measured with a precision of 1%. Resolution of the device must, therefore, exceed one part in 10^4 parts. Furthermore, since the measurement is in the time domain and the scanning period is typically 10^{-5} sec, then time of intercept data precision of $> 10^{-9}$ sec is necessary. The relationships between the scanning waveforms and the return signals are shown diagrammatically in Figure 8.

In order to obtain a maximum resolution of 1 part in 10^4 parts, there must exist at least that many resolvable "spots" per gage length. Since the motion of a laser scan spot past a stationary reflective edge yields a signal approximating a Gaussian distribution, rather than a step function, the position of a singular scan spot may be ascertained to better than one tenth of a spot diameter. Therefore, to achieve the required resolution, a laser spot diameter of approximately 10 microns was chosen.

Actual experiments were conducted with a 40 micron spot diameter and the results were marginal; the available laser power was insufficient to generate a favorable signal-to-noise ratio. The instrument is, therefore, only capable of 10^3 resolvable spots in a 1 cm gage section with the present 10 mw, 4880 Å laser, utilizing 100 micron apertures.

It is obvious that the greater the difference in emissivity between the coated area and that of the substrate, edge identification is easier. From Figure 8, it is also evident that the greater the slope of the signal voltage (dv/dt) at t intercept, the greater the precision of the measurement. Typical uncertainties of < 0.01% are encountered in the intercept time measurements.

Laser Scanning Technique

The scanning subsystem was by far the most problematical in development of the system. Scanning a light beam over a subtended angle of one degree at rates exceeding 10^5 Hz is difficult. Several approaches to the problem were taken. A brief review of scanning techniques is presented in Table I.

Table I

Review of Laser Beam Scanning Technique

Scanning Technique	Mode of Operation	Relative Cost	Bandwidth Limit
1 Rotating Quartz or Be mirror	Multiple reflection from moving facets	Low	50 KHz
2 Light beam galvanometer	D'arsonval mirror movement (low inertia)	Moderate	30 KHz
3 Piezo-mirror	Piezo-electrically moved reflecting surface	Moderate	20 KHz
4 $LiNBO_3$ e.o. refractive cell	Change in n, with applied field	High	50 MHz
5 Liquid refractive cell	Change in n, by induced acoustic wave	Moderate	1 MHz
6 HIO_3 electro-acoustic cell	Bragg diffraction	High	1 MHz (at present)
7 Pb Mo O_4 e.o. electro-acoustic cell	Bragg diffraction	High	1 MHz (at present)

At this time a high speed optical galvanometer is performing adequately while only capable of a 50 KHz scanning rate. The frequency response may be extended by overdriving the device. However, linearity and reliability suffer. While ideally the scan wave form should be triangular, some rounding of the peaks will always be experienced because of inertial damping of the device. As seen in Figure 10 the triangular waveform may be synthesized by adding to a fundamental sinusoidal wave an infinite number of harmonic waves of diminishing amplitude. While the highest input frequency may fall far beyond the flat frequency response of the galvanometer, the harmonic frequencies are rapidly diminishing in amplitude. The amount of frequency distortion contributed by inadequate flat frequency response (of the galvanometer) may be of minor significance. Actual experiments show that 80% of the scan period is useful at this rate. Use of the lead niobate diffractive scanner (see Table I) will ultimately extend the frequency response of the extensometer to the sub-millisecond region while still maintaining adequate resolution.

Receiving Optics

Since the reflectivities of the typical test specimens are relatively low, and the laser beam power is in the milliwatt region, a fast optical train is important.

A special 2-20 power F:8 zcom "telescope" was designed and manufactured by Zoomar, Inc., Glen Cove, New York, which will permit the target area on the test specimen to nominally fill the sensitive area of the photomultiplier tube thereby gaining a more favorable noise figure. The lack of focusing adjustments (with a fixed working distance of 80 cm) permits any size target to be examined. On materials which exhibit

relatively low strains, the magnification can be increased, thereby increasing spot resolution. Provisions are made for narrow band filters, which are placed immediately behind the collimating lenses on the telescope.

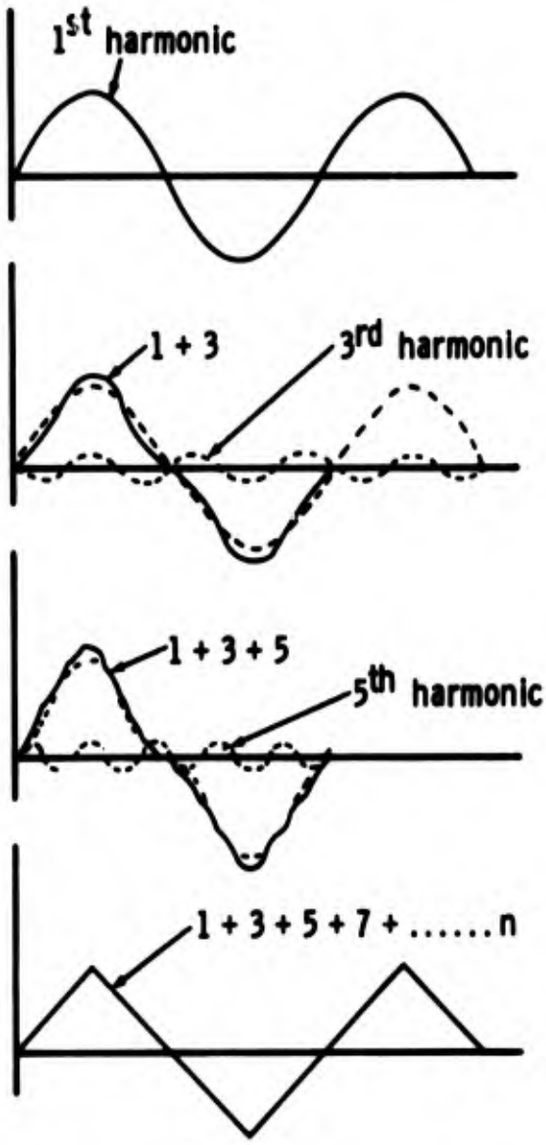

$$f(x) = \sin x - 1/9 \sin 3x + 1/25 \sin 5x - 1/49 \sin 7x + \ldots\ldots 1/N^2 n$$

Figure 10 Fourier Representation of Triangular Wave

The optical system (Figure 11) is colinear in transmitting and receiving optics, thereby permitting the whole device to be repositioned without the necessity of realignment. A small elliptical diagonal mirror placed in the center of the objective accomplishes this.

As seen in Figure 11 the laser beam passes through diffraction limiting pin-hole apertures (b) from where the beam impinges upon the optical galvanometer (c). The scanned beam then passes through a beam rotator (d) which consists of a crown glass dove prism allowing the scan raster to be rotated 90° to accommodate either vertical or horizontal targets. After reflection from a kinematically mounted mirror (e), the beam strikes the diagonal first surface reflector (f) and illuminates the specimen (g).

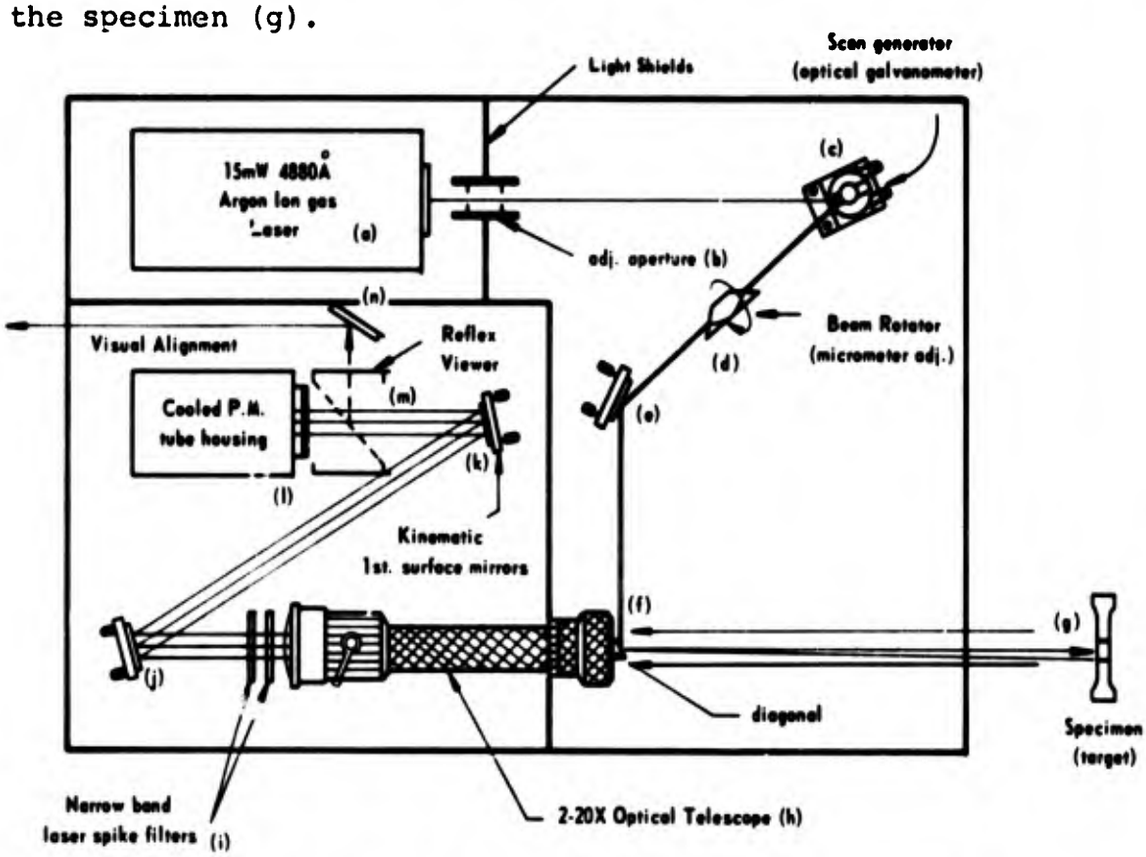

Figure 11 Schematic of Scanning Laser Extensometer

The reflected laser light is gathered by the input optics (h), passed through the frequency selective narrow band filters (i) and then off two kinematically mounted mirrors (j,k) onto the photomultiplier face (l). A reflex viewer is interposed between the P. M. tube and second reflector. The reflex viewer serves as an alignment tool during setup; after which only the beam position on the specimen gage section need be verified. In use, the pneumatically-actuated reflex viewing mirror is locked up, thereby obscuring any light leakage through the viewing telescope and ground glass. To aid during alignment, the two selectable narrow band filters are mounted in a pneumatically-actuated carriage which may be moved.

While the preponderance of kinematic mirror mounts may seem superflous, they greatly simplify the alignment procedure. An alternate technique for producing micron-size spot sizes on the specimen involves more optics but significantly improves system performance. The present 0.5 mm diameter laser beam would be expanded to nominal 1 cm diameter with a Galilean beam expanding telescope. The expanded beam is now scanned by the diffractive $PbNbO_3$ cell. A post focusing field lens would focus the scanned beam onto the specimen. Since the beam spot resolution is inversely proportional to the lens "f" number, and the effective aperture is fixed at 1 cm, the physical problems of mounting the lens close to the specimen would be difficult.

Photomultiplier System

In order to optimize the sensitivity of the receiving system, a photomultiplier tube was selected which would exhibit a high

sensitivity at the operating wave length of 4880 Å. An RCA 8575 P. M. tube was selected. The bialkali photocathode provides an absolute sensitivity of over 50 mA/watt; the high quantum efficiency, 12 stage tube has a 2" diameter end-on window. An anode dark current of several nano-amperes can be further reduced by operating the tube at -20°C in a cooled housing. When operated at an anode-to-cathode voltage of 2000 volts, the tube is capable of a luminous sensitivity of 300 amp/lumen.

The thermoelectrically cooled housing provides electrostatic and magnetic shielding as well as housing the divider network. A combination power supply and electrometer amplifier provide some flexibility in operation by permitting optimization for static conditions. The output for the signal processing gear for dynamic measurement is taken directly off the anode of the tube.

If the smaller apertures (10 micron) are employed with the present power-limited laser, a new gallium-phosphide (Quantacon type) P. M. tube may be necessary. These new tubes provide an order of magnitude improvement in sensitivity while not materially affecting spectral response or dark noise characteristics.

Mounting

The entire extensometer is mounted on an aluminum alloy table which serves to damp out any high frequency vibrations. A light-tight aluminum cover which houses the reflex viewing optics is easily removed.

The table rests upon a fully adjustable mount which provides fore and aft focusing movements as well as angle adjustments. A fairly large thrust bearing allows smooth rotational adjustment (through a worm gear) while a television camera pedestal provides motorized elevation control. Still missing is a base lock-up mechanism which would further isolate the extensometer from the environment. Expanding the beam to a larger initial diameter would help maintain a low "f" system; however, the clear aperture of the diffractive scanning cell would have to be increased proportionately. A more satisfactory solution may be possible by operating off axis thereby not interfering with the receiving optics. The above constitute changes which might be made in a second generation laser extensometer.

R. F. SPUTTERING OF STRAIN GAGE SECTIONS

The use of the laser extensometer previously described depends on being able to reflect the laser beam off the specimen surface. This technique is very successful as long as the specimen surface remains in a condition to accurately reflect the laser beam without any distortion other than that produced by straining. However, a problem develops in testing materials like graphite and carbon phenolic because the surface distorts on heating. This distortion takes place at such a rapid rate that the straining effect is masked. Thus the laser extensometer receives a pattern that represents the effect of radiant surface energy distortion and mechanical straining. The other methods of measuring strain have already been discussed and dismissed as being unusable in this application. Therefore, the problem becomes one of finding a technique to obtain a surface that will be reflective at the temperatures (> 6000°F) involved and that will represent what is occurring in the bulk of the specimen. One solution is to somehow coat

the surface with a thin film which maintains itself at the temperature and yet is thin enough not to change the bulk specimen properties being measured.

Many techniques are currently being utilized to place thin coatings on substrate materials. Generally these methods can be divided into two catagories based on the kinetic energy of the arrival atoms. On the basis of energetics considerations, the coating methods can be divided into (a) low energy deposition (chemical vapor deposition, flash evaporation, etc.); and (b) the high energy or plasma deposition methods (d-c, r.f. sputtering, and ion plating). The film formation and type of interface depends largely on the kinetic energy of the arriving atoms. Adhesion characteristics of a deposited film to the surface are known to be dependent on the type and structure of the interfacial region. A comparison of the film formation characteristics which have been deposited by both low and high energy deposition methods would be beneficial.

Chemical vapor deposition may be defined as condensation of an element or compound from the vapor phase to form a solid film. The coating material is melted and vaporized under vacuum, generally. The film formation then occurs by nucleation of the vapor and by grain growth. The substrate surface has preferred sites where nuclei develop into islands which then grow both normal and horizontal to the surface. Finally the islands coalesce to form the continuous, two dimensional medium which is considered to be the thin film.[9] The substrate temperature is one of the most important parameters, for in order to achieve good adherence, diffusion is necessary. In vapor deposition techniques, the evaporated atoms have only thermal energy (approximately 0.1 to 1.0 ev.).[10] Consequently,

film adherence depends on forming a good chemical bond between the deposited vapor and the substrate. Diffusion is, therefore, necessary to form the chemical bond, and diffusion depends on (1) the size of the diffusing atoms, (2) the temperature of diffusion, and (3) mutual solubility of the atoms involved.[11]

In contrast to vapor deposition, the high energy or plasma deposition process of sputtering have energies to 100 ev, depending on the potential between the electrodes. In its simplest form physical sputtering is the removal of surface materials from a solid by ion bombardment. This is usually accomplished in a low pressure d.c. or r.f. discharge by making the material to be sputtered the cathode (target) and the substrate holder the anode (Figure 12). A negative voltage applied to the cathode creates a glow discharge or plasma within the interelectrode spacing. The positive ions of the plasma, upon striking the cathode with sufficient momentum to overcome the intrinsic bonding energy of the lattic atoms, will enable surface atoms to be ejected from the cathode. The sputtered cathode atoms are then propelled to the anode or substrate where the desired thin film is achieved.[10]

Film formation during sputtering does not occur by the process of evaporation and condensation. In sputtering, the sputtered atoms are physically disengaged or knocked off by impact of the accelerating argon ions. The sputtered atoms are transferred to a surface by a momentum transfer process. When the sputtered atoms strike a cold surface, a continuous film forms from the very beginning, contrary to the island formation during nucleation of the low energy deposition.[12]

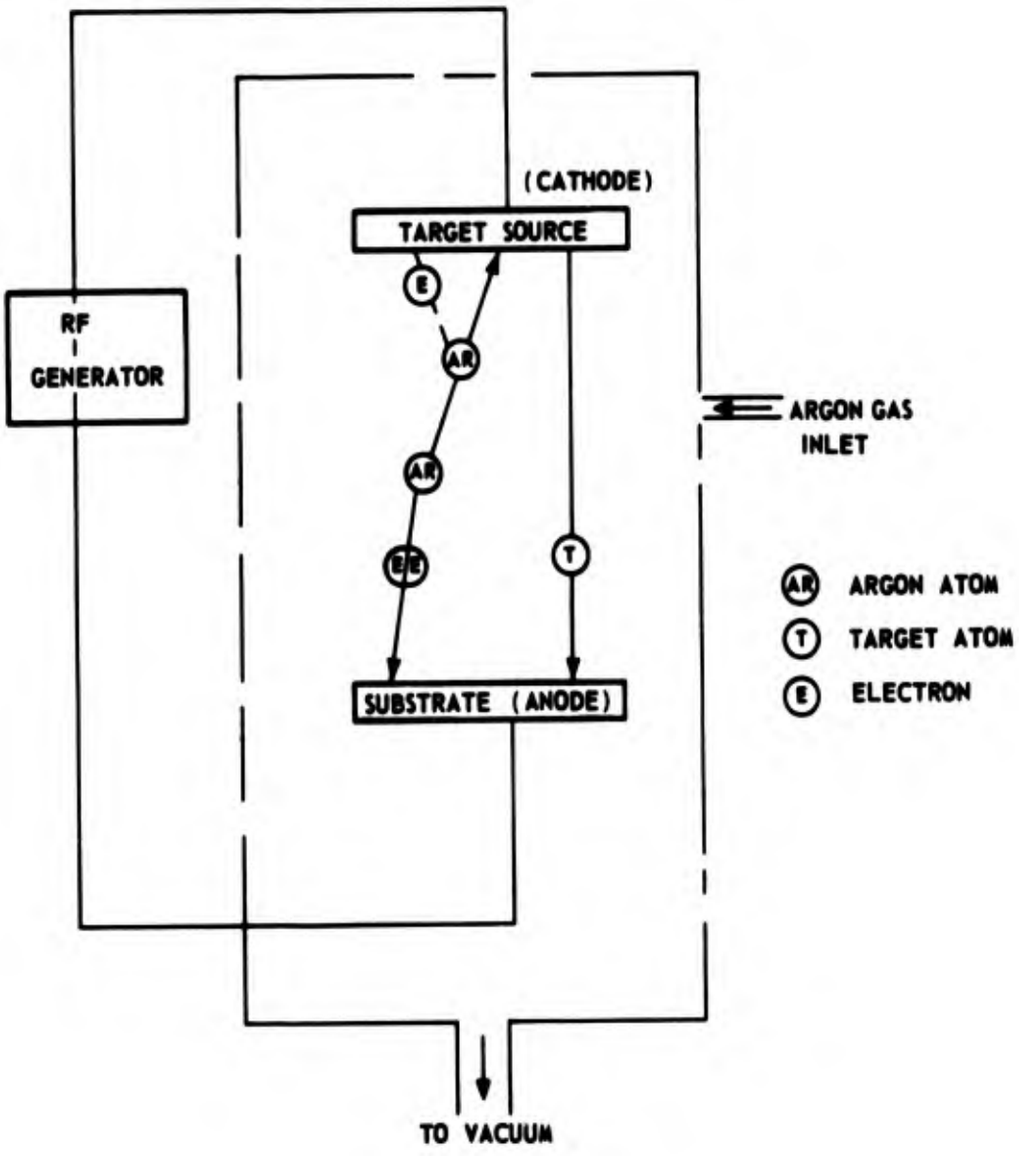

Figure 12 Schematic Representation of r.f. Sputtering

Another sputtering technique developed very recently vastly improves the adhesion between the sputtered target atoms and the substrate material. This technique is called bias sputtering. Previously the power was directed by means of a switching circuit either 100% power to etch or 100% power to sputter the target atom. In the bias technique, a power dividing circuit is used to start with the power in 100% substrate etch, and gradually the power is transferred to the target until the target reaches full 100% power (Figure 13).

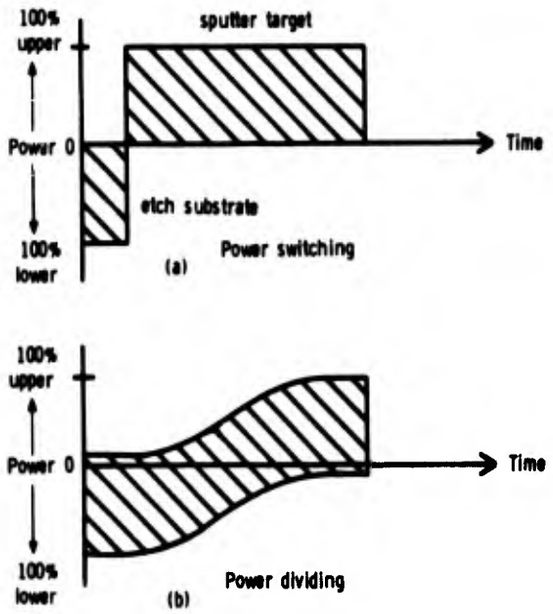

Figure 13 Two Modes of Sputter - Etching

This permits a continuous scrubbing of the deposited film. The coated substrate now consists of (1) 100% substrate atom, (2) a transition coating of 99% substrate atoms and 1% target atoms to 1% substrate atoms and 99% target atoms, and (3) 100% target atoms. The adhesion is vastly improved since the target atoms and the substrate atoms are interdispersed. The bonding, therefore, takes place over several hundred times the distance as in the power switching case; i.e., from 200 Å to 1000 Å approximately.

In order to get best results during sputtering, the system must be in a right set of complex combinations of impedances. For maximum power transfer from generator to load, the stray resistances, capacitances, and inductances should be minimized. Even more importantly, these parameters, once minimized, must be kept constant so that the electrical parameters of the discharge can be controlled accurately.[13]

Materials to be sputtered are very important to any r.f. sputtering configuration. The exact mechanism by which a material is emitted varies somewhat depending on the target material. It is fairly well established that momentum transfer from the fast moving positive ions attracted from the discharge toward the target surface causes rupture of the target surface bonds. The elastic constants of the targets and the strength of the atomic or molecular bonds in the target materials are the important parameters.

Sputtering rates depend on the exact target material. Elemental metals have the highest sputtering rate with their alloys somewhat lower. Insulators have been grouped into three classes: (1) Simple crystalline solids (SiO_2, Al_2O_3), (2) multicompound crystalline solids ($BaTiO_3$, 2CdO, Nb_2O_5), and (3) noncrystalline solids (glasses). Of the three, noncrystalline solids have the highest sputtering rates and multi-compound crystalline solids the lowest.

One problem of the thin film is the resulting structure.[14] Nearly all materials sputter stoichiometrically identical to the target materials but the structure is undensified and the bond angles are different than the bulk materials.

Unfortunately, this is somewhat true of all deposition techniques such as vapor deposition. Films are found not to have their theoretical bulk density and are usually amphorous as sputtered (deposited). Heating either during or after deposition corrects most of these deficiences. The energy of the sputtered species upon arrival at the substrate is quite high, causing the substrate temperature to rise. If the substrate is also heated, sublimation from the substrate may occur.

The r.f. sputtering equipment obtained to complete this program (Figure 14) consists of a 2-5" water-cooled target configuration with a substrate etcher. The double tuned transformer-coupled output is an invaluable aid in achieving stability on

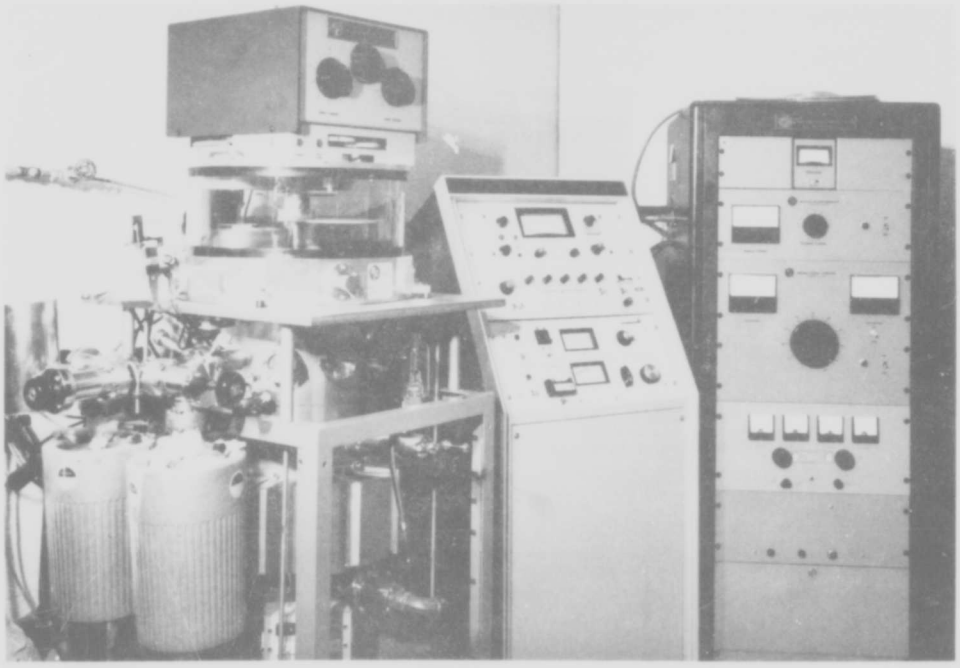

Figure 14 Photograph of r.f. Sputtering Equipment

long sputtering runs. The r.f. generator operates at 13.560 MHz, which is the only FCC allowed frequency that is suitable for sputtering. In order to achieve a suitable vacuum, a series of vacuum pumps are used: 2 stage mechanical pump with foreline trap, 4 sorption pumps, 400 ℓ/sec ion pump, and a titanium sublimator to getter oxygen and water vapor. With this combination, a pressure of 5×10^{-7} torrs is attainable in a reasonable time with a clean vacuum system.

Based on the success of r.f. sputtering, the technique when applied to the graphite specimens gave a surface which is be reflective at the temperatures required. Films of hafnium were sputtered onto the specimens by the following procedure (see Figure 15):

1. A brass mask was constructed to give the area for the laser beam to focus upon.

2. System was evacuated for 14 hours at a pressure of 1×10^{-5} torrs.

3. Pressure was reduced to 8×10^{-7} torr for 30 minutes and the system was purged with pure dry argon.

4. Argon was emitted into the system and a titanium getter absorbed any reactive gases like oxygen or water vapor.

5. With argon pressure at 3 microns, the power was applied and sputtering at a rate of 500 Å/min. took place for ten minutes. The film thickness was measured to be 5000 Å.

6. The power was turned off and the specimens remained in the argon atmosphere for one hour to stabilize.

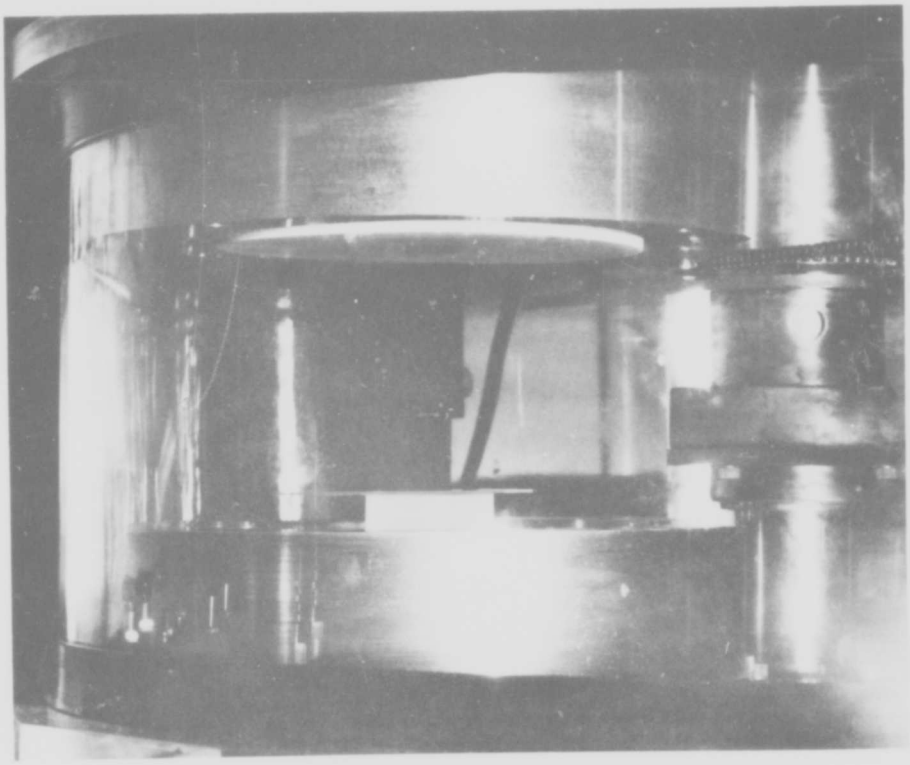

Figure 15 Photograph of Sputtering Process

HIGH TEMPERATURE MEASUREMENT

During the course of the high temperature testing program, tensile test specimens of ATJ-S graphite and RAD 6300 carbon phenolic were heated to temperatures in excess of 6000°F. Tests were performed in both vacuum (< 20 microns Hg.) and argon gas (15-20 psi).

Instrumentation used for specimen temperature measurement consisted of an automatic monochromatic optical pyrometer (Pyrometer Instrument Co., Inc., Pyro Photomatic Pyrometer #A-144) and an infrared radiometric microscope (Barnes Engineering Co., Model RM-2A). Platinum-rhodium thermocouples were used for low temperature correlations while hafnium, iridium, and tantalum metals were used for high temperature melting point calibrations.

The automatic optical pyrometer is essentially an auto-nulling servo version of the classical disappearing filament pyrometer. The internal optics permit the device to examine an area within a 0.040" spot at a working distance of approximately 12". While the precision, drift and accuracy of the calibrated pyrometer are indeed commendable (Figure 16), the use of three definite scales (1450°F - 2500°F, 2400°F - 3800°F, and 3600°F - 7200°F) does not permit continuous, uninterrupted temperature measurement without scale switching and the attendant loss of time.

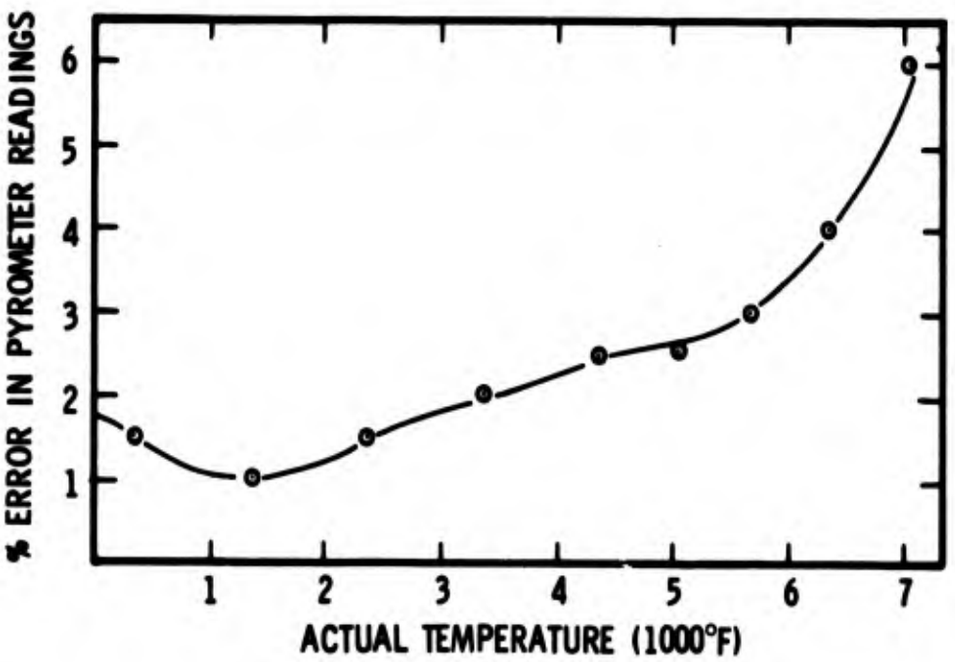

Figure 16 Automatic Optical Pyrometer Reading Error - Calibrated on a Blackbody

To this end, the radiometric microscope was used as a continous indicating and recording instrument throughout the heating period. While the microscope is no longer inherently calibrated when equipped with a radiation attenuator (to extend the useful range to temperatures in excess of 6000°F) the readings may easily be correlated by using the optical pyrometer as a reference standard.

When heating times on the order of tens of seconds were required, the optical pyrometer was normally used (since there was adequate time to switch ranges) and the 100 millisecond servo response time was adequate. At higher heating rates (100 to > 1000°F/sec) the radiometric microscope was generally used. Since the output of the solid state detector is logarithmic with increasing temperature, scale compression and accuracy at lower temperatures (up to approximately 1000°F) suffers. To decrease the dynamic range of the device one simply adjusts the input aperture, thereby increasing low temperature resolution.

The automatic optical pyrometer was calibrated according to N.B.S. test procedures and typically exhibited a confidence level (95%) of better than 0.2% at any temperature within the range of interest. It is important to realize that such a high confidence level is only possible with blackbody sources or when the most rigorous procedures are applied to the system under examination to determine spectral emissivities.

An additional consideration is the variation in spectral emissivity with temperature; a source (specimen) at an assumed temperature of 4500°F with an emissivity of 0.90 will actually be at a temperature of 4850°F should the emissivity change to

0.70 and the radiant output remain constant. At temperatures in excess of 5000°F the surface structure of specimens changed drastically in relatively short periods of time, thereby altering emissivities. Increased vapor pressures and diffusion coefficients were primarily responsible for such instabilities. Obviously, if emissivity is a function of temperature, time, and gaseous environment, the measurement and determination of true temperature is highly complicated.

Further complications such as obscuring condensation products on quartz sighting windows and the peculiar asymmetry of the graphitic composites, necessitated "in situ" calibrations of the system. To this end, calibration techniques which could readily be incorporated in the testing device were attempted. Several test specimens were equipped with small cavities drilled perpendicular to the major axis. These cavities (nominal 0.08" dia. x 0.18" deep) served as small blackbody reference cells which could be used to accertain true specimen temperature and surface emittances. The readings derived by this technique were not accurate, however, because of the attenuating windows, etc. Therefore, melting point calibrations were run with slivers of hafnium, iridium, and tantalum metals (all > 99.99% purity) inserted into the "black" cavities. The melting points were visually determined and correlated to the indicated surface temperature. These figures were then used as the correction factors for future test runs.

Performing melting point calibrations is generally a fairly straightforward way of calibrating the overall system. However, since most of the test specimens in this program consisted of either graphite or a graphite-bearing material, severe limitations were imposed as to which materials should

be used for melting point determinations. Very few high melting point materials do not form carbides when heated in an atmosphere of carbon vapor (i.e. the small black cavities); furthermore, even fewer materials form carbides which have melting points above the melting point of the starting element or compound. Among the noteable exceptions are hafnium and tantalum, whose carbides are nominally stable to temperature in the 7000°F region. Iridium does not readily form a carbide, but a melting point of approximately 4400°F does not provide a very high temperature reference point. Figure 17 shows some of the melting point derived temperature values for the radiometer. Figure 18 is a correction curve used for the test results in Section II for two values of emissivity.

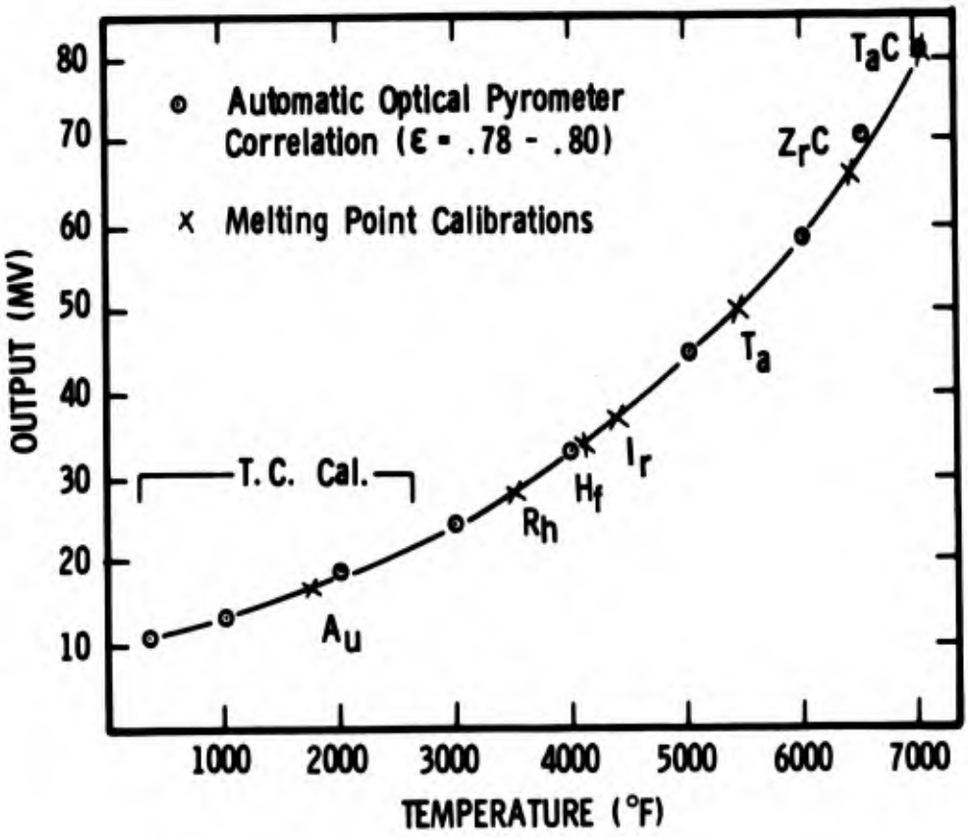

Figure 17 Radiometric Microscope Output

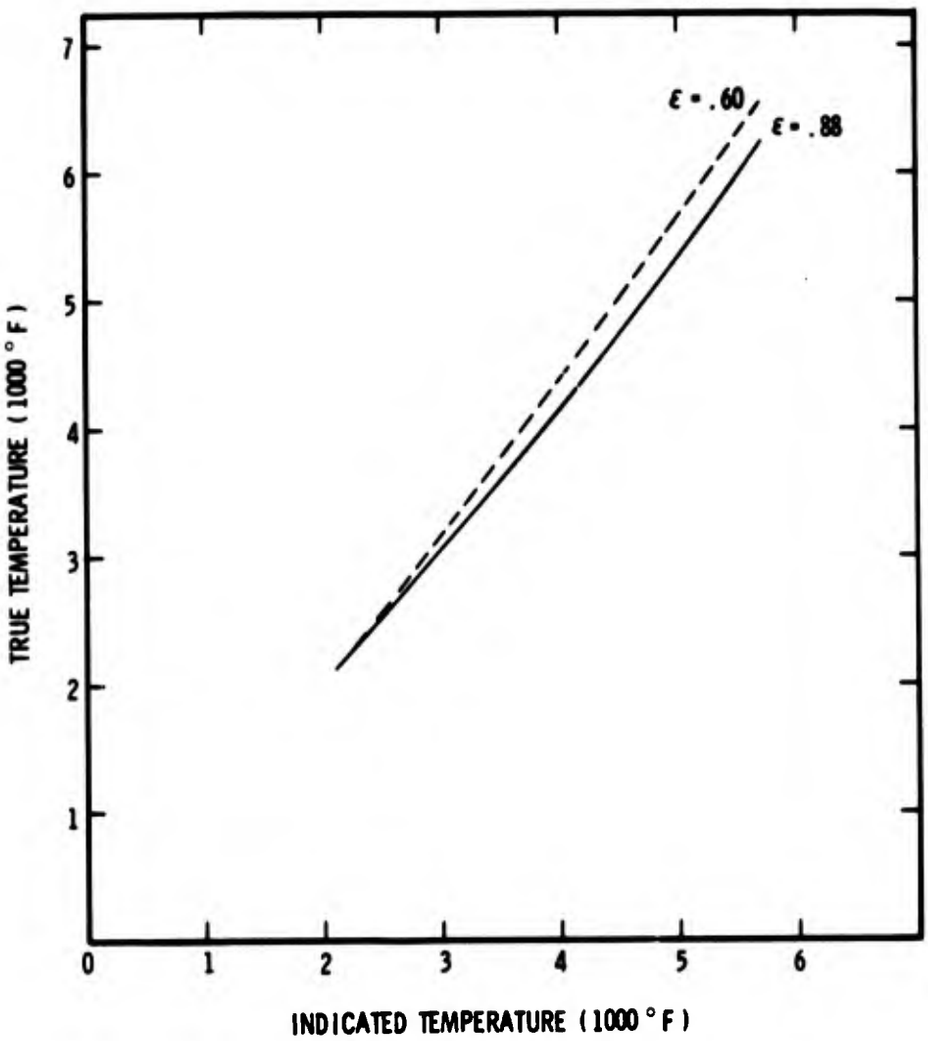

Figure 18 Temperature Correction Curve

An inherently absolute calibration procedure was attempted early in the program. A sensitive spectroradiometer scanned the wavelength spectrum emitted by the hot specimen and recorded irradiance versus wavelength. By applying Wiens displacement law (discussed in Reference 1) to the experimental data, the actual temperature (color temperature) could then

be determined. It was discovered, however, that the non-linear response of the photodetector in the region of interest--1.50 microns to 0.75 microns or 3000°F to 6500°F (see Figure 6)--masked the relatively subtile difference in radiant output about a narrow spectral region.

SECTION II
EXPERIMENTAL RESULTS AND DISCUSSION

INTRODUCTION

Two materials were characterized in uniaxial tension:

Graphite (ATJ-S)*

A polycrystalline, fine grain, premium quality, synthetic graphite, it is made from mixing petroleum coke with pitch and pressure molding into a billet shape. ATJ-S grade is characterized by being reimpregnated with special organic materials under high pressure.[15] Although not determined for each test specimen, density measurements were made on the raw 8 inch diameter by 7-inch long billets as well as sample cores taken from the billets from which test specimens were machined. The average density was determined to be 1.83 gm/cm^3. Extremes of 1.86 and 1.80 gm/cm^3 were measured.

Carbon Phenolic (RAD 6300)

A high quality carbon phenolic, this material was compression molded into panels 12 inch by 12 inch by 3.75 inch thick. Pluton B-1 carbon fabric (3M) was preimpregnated by Fiberite Corporation (Winona, Minnesota) with SC-1008 phenolic resin (Monsanto). Reinhold Aerospace Division of Haveg Industries (Santa Fe Springs, California) molded the panels from which tests specimens were machined. Nominal bulk density of the panels was 1.40 gm/cm^3, giving a resin volume fraction of about 50%.

---

* Manufactured by Union Carbide Corporation

Tensile specimens (see Figure 19) were machined parallel to the billet axis (or across the grain) for the graphite and parallel to the warp (fiber) direction for the carbon phenolic. Grinding techniques were used in order to maintain close tolerances on specimen concentricity and cone angles to assure uniaxial loading in the test machine.

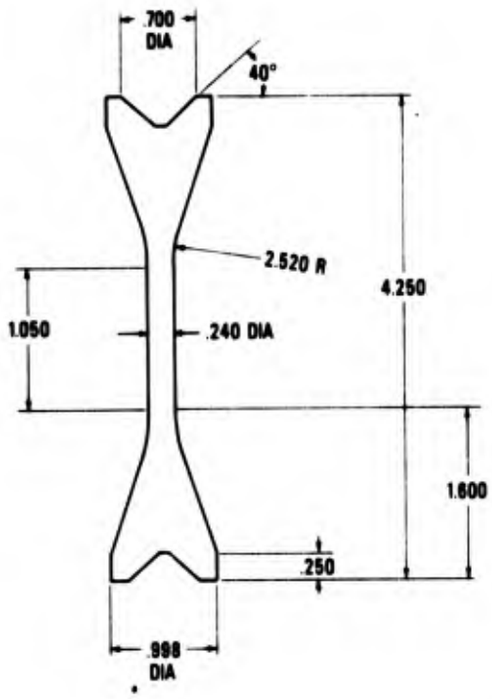

Figure 19 High Temperature Test Specimen

Temperature profile tests were conducted in order to determine gradients in a tensile sample at various test temperatures. At a 5000°F central section temperature measured with the optical pyrometer, the specimen interior temperature was within 100°F using tungsten-rhenium thermocouples. This 5000°F surface temperature was constant approximately over the center 1.25 inches. Gradients near 3000°F were measured in the grip contact area. This large temperature gradient served

to protect the jaws of the grips which are in direct contact with the specimen. Accuracy of surface temperature measurements above about 4000°F is discussed in the Description of Test Technique Section of this report.

Test results are presented as tensile fracture stress versus temperature after various heating rates and/or hold times at temperature. Since the primary objective of this program was to study the time-temperature behavior of these two materials, all of the test loading times were nearly constant at between 10 and 30 milliseconds. This nominally gives strain rates from 1 to 10/sec, depending on the material and test temperature.

As discussed in the Description of Test Technique Section, measuring strain directly in the specimen gage section is extremely difficult at high temperatures and strain rates. Part of this program involved developing a new technique to accomplish this objective. Unfortunately, time did not permit the use of the device under all test conditions. Therefore, as an alternate method of measuring strain, an optical tracker was used to measure the lower grip motion on the test machine. Then an "effective" gage length was determined at room temperature and used to determine strain from the lower grip motion. To determine this "effective" gage length, strain gages were mounted in the center of the constant cross section of a tensile specimen. In addition to the strain gages, a painted gage section was placed in the same area and tracked with an optical extensometer. These two methods were used to measure dynamic strain while the lower grip motion during the same test was monitored. By comparing the displacement of the lower grip to the strain measured by the strain gages and

optical extensometer, an "effective" gage length can be determined as follows:

$$l_{eff} = D/\varepsilon$$

where: l_{eff} = effective gage length

D = lower grip displacement

ε = strain measured by strain gages or optical extensometer

Tests were conducted on carbon phenolic and are shown in Figure 20. This figure shows the stress-strain results of two tests after the "effective" gage length was calculated. Excellent agreement was found for an l_{eff} = 4.25 inches. It is interesting to note that 4.25 inches is the total specimen length. This result is not unusual considering the small strains to fracture that were measured. In addition, the linear elastic brittle characteristic of this material (at least at room temperature) would reduce the tendency for localized strain or necking; thus, strain occurs throughout the specimen length. One other factor is worth mentioning. Although the load required to fail this material was small (near 400 lb.), some slight amount of machine stretch does occur. This is primarily in the grips and preloading mechanisms, thus adding to the measured lower grip displacement. While these "effective" gage length tests were only conducted on carbon phenolic at room temperature, the results should be useful for determining strain on the graphite since failure loads and strains are similar. Use of this technique at elevated temperatures is less optimistic. As long as the material behaves in a brittle manner, results should be nearly as accurate as at room temperature. Even so, it should be noted that this technique for measuring strain is not a direct method (such as using the laser extensometer). Therefore, caution should be used

when interpreting the strain data. A conservative estimate of strain accuracy reported in this work would be ± 30%.

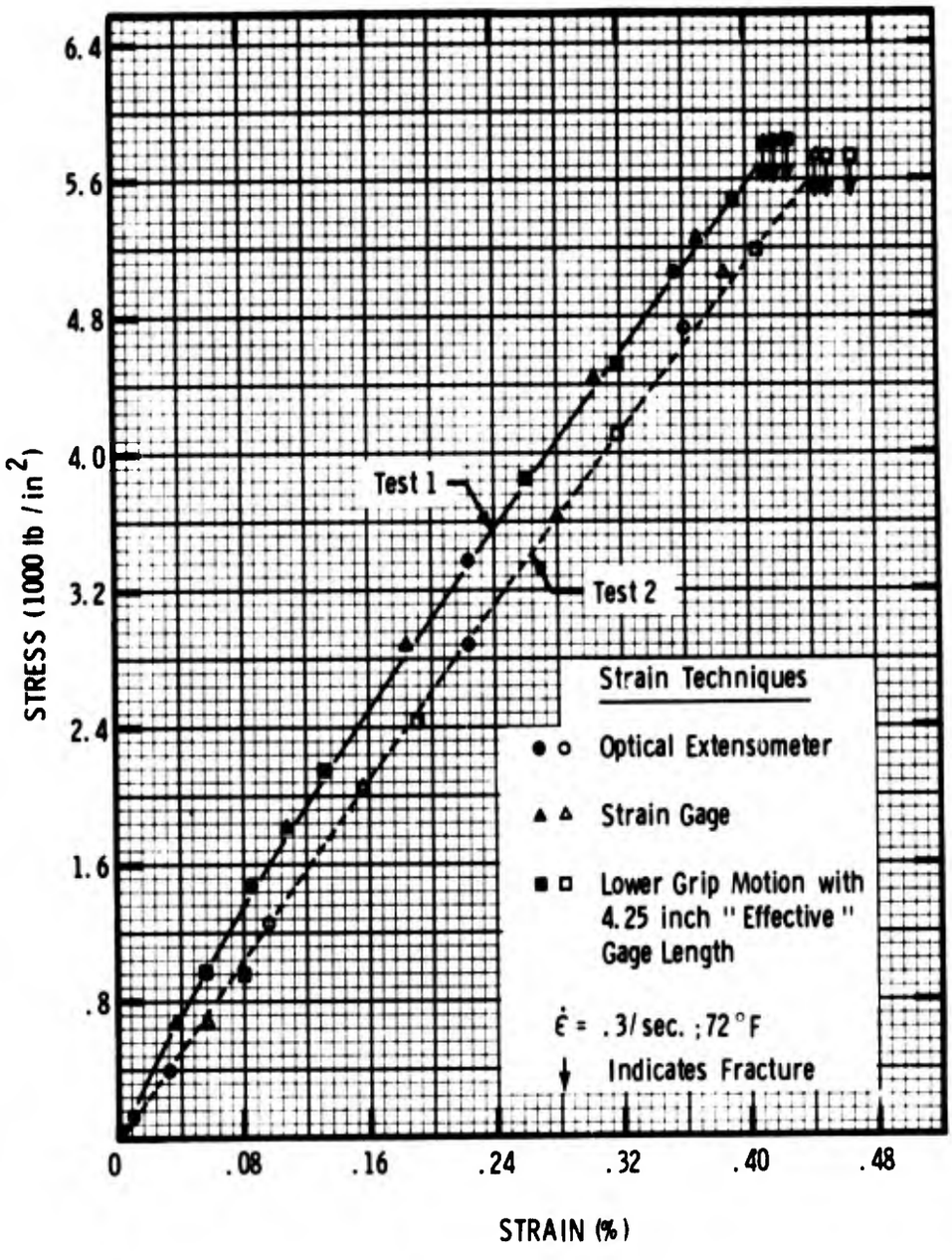

Figure 20 Effective Gage Length Calibration

GRAPHITE (ATJ-S)

Figure 21 shows the results of tensile tests on ATJ-S graphite, where fracture stress is plotted against test temperature. Heating rates of 10 to 1000°F/second were examined, where immediately upon reaching temperature the test machine was triggered to start. In addition, results are shown from tests where ten second soak times were attained prior to testing. Tensile specimen axis was taken parallel to the billet axis, or "across the grain" of the graphite. No distinction was made as to the radial location of each specimen on the 8 inch billet diameter.

Plotted in Figure 21 are average data points from at least three tests at each condition with the maximum scatter in fracture stress shown as vertical error bars. The horizontal error bars represent the maximum probable error in temperature if the assumed surface emissivity were incorrect. The temperature associated with each average data point is a corrected temperature from the measured value (see Figure 18). This correction includes a pyrometer blackbody correction, a quartz vacuum jar viewing window correction, and a specimen surface emissivity correction where $\varepsilon = 0.88$ was assumed. The temperature error bar indicates the true temperature if the emissivity was actually 0.65 and all other corrections were the same as for $\varepsilon = 0.88$.

These results show that the effect of heating rate on fracture stress (at least up to 1000°F/sec) is negligible up to temperature near 5500°F. In other words, material scatter overshadows any other effect. Above this temperature, time effects become important. In Figure 21, the dashed line represents a compilation of data[5,15,16] on ATJ-S graphite where heating rates

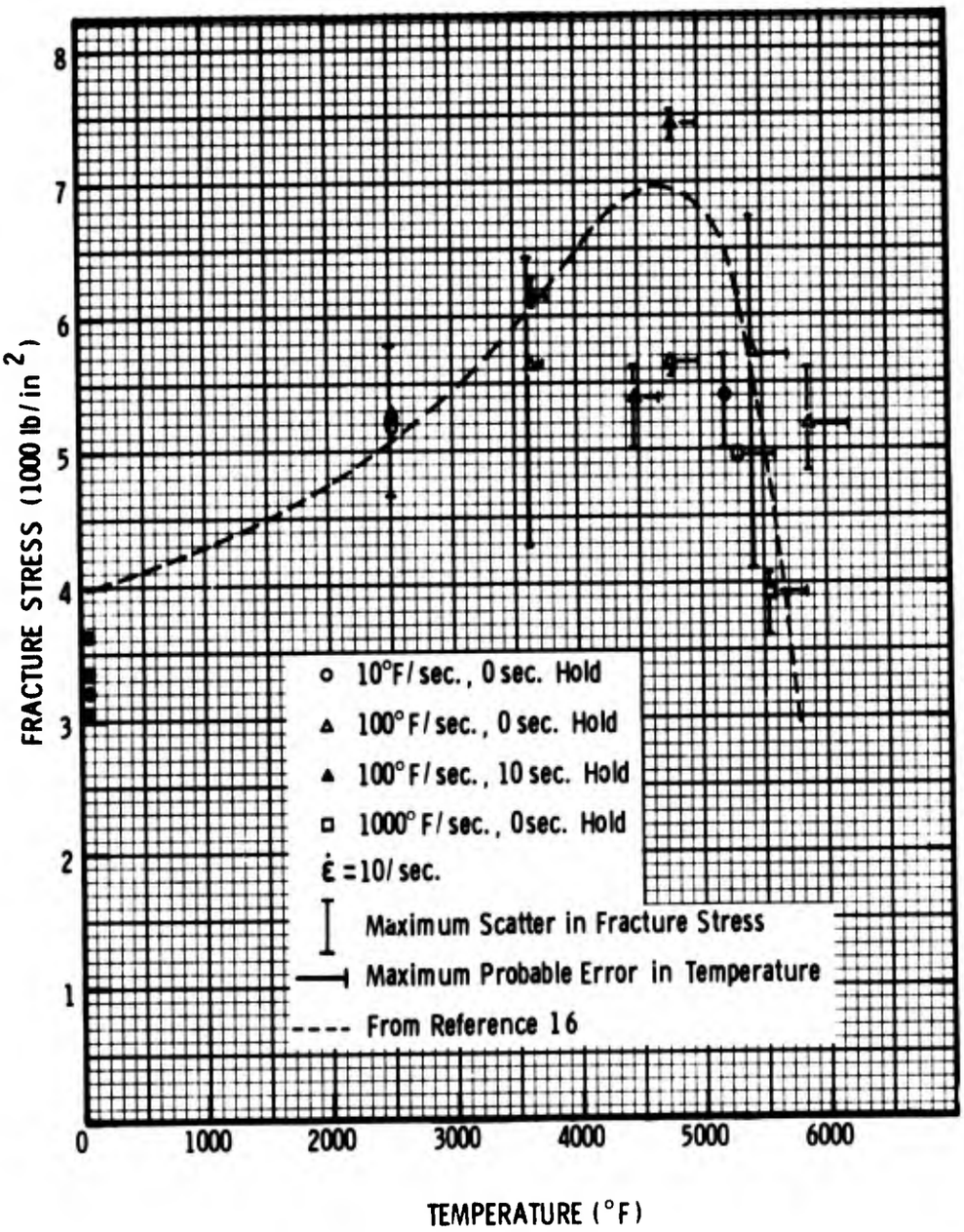

Figure 21 Fracture Stress Versus Temperature for ATJ-S Graphite

were lower, times-at-temperature were longer (near 20 minutes), and strain rates were lower. Even though very little oxygen was present in the test chamber (in fact, in most of the tests at temperatures above 5500°F an argon atmosphere was introduced in the test chamber), preferential oxidation and sublimation took place on the surface of the specimen which created small pores or pits. In addition, graphite crystal growth was observed in specimens heated to near 6200°F (Figure 22). The observed microscopic increase in porosity throughout the specimen from samples sectioned after cooling to room temperature may be due to localized sublimation. The number of these pores produced is a function of time, thus causing the cross sectional area of the sample to decrease with time. This phenomenon is similar to necking in a ductile metal, where true stress and not engineering stress is required to interpret the results. Thus in these graphite tests, original cross section is not a valid constant in determining tensile strength.

The laser extensometer, discussed in the Description of Test Technique Section, was not completed in time to perform any valid tests in this program. Although lower grip displacement was measured in most of the tests, there was a lack of consistancy in the strain measurements. The only conclusion that can be made is the strain-to-fracture increases above about 4500°F. This observation is consistent with others.[16]

The increase in strength of graphite with temperature up to about 4500°F has been explained by several authors. Mrozowski[17] early proposed that the observed increase in strength and modulus is due to a temperature relieving of locked-in stresses between grist and binder particles caused by cooling from the cure temperature. Martens, Jaffe, and Jepson[2] proposed that the increase was due to an increase in ductility caused by porosity

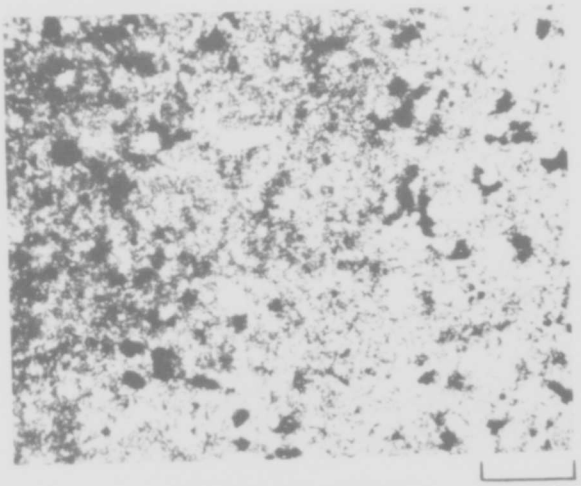

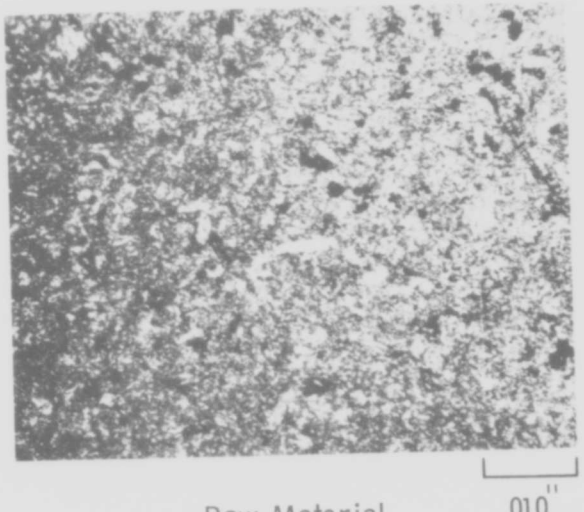

Figure 22 Photomicrographs of ATJ-S Graphite

reduced stress concentrations. Diefendorf[18] found the increase in strength was partly from stress relieving and partly from an atmospheric effect. He found that at temperatures up to about 4000°F, introduction of an argon atmosphere reduced fracture strength unless the deformation speed was increased, where the effect was minimized. The effect was described as a stress corrosion phenomenon, where tensile deformation stretched the bonds between basal planes thus making them vulnerable to chemical attack by the gas. Smith[19] found that a 3 psig helium atmosphere reduced fracture strength nearly 25% at 3700°F and a low strain rate. An increase of strain rate by three orders of magnitude reduced the atmospheric effect as seen by Diefendorf. Gillin[20] suggested that the observed higher fracture stress in vacuum[18] was due to an increase in the coefficient of friction on the basal planes. He proposed that the increase in strength with temperature is caused by elimination of stress concentrations at tilt boundaries in the grist particles which were found to act as barriers to dislocation motion.

Although most of the "open literature" investigations on graphite limited the maximum temperature to near 4500°F, some of the observed behavior from the present program at higher temperatures can be explained by these theories. For instance, in order to increase the sublimation temperature a 20 psig argon atmosphere was introduced for tests above 5000°F. The argon did permit testing at higher temperatures (thus increasing the sublimation temperature) but had no effect on fracture stress up to 5500°F. This observation is consistent with Diefendorf[18] and Smith[19] since the test times were extremely short in these tests (10-30 msec).

Since the primary purpose of this study was to determine the effect of heating rate and/or time-at-temperature, specimen loading time was kept short. A few tests were conducted at 3500°F at a lower strain rate (loading time about 5-10 seconds). These results are not included in Figure 21, but fracture stress was within the scatter shown in the figure. This observation is somewhat different from that of Hale and Fassell,[6] Smith,[19] and Green, Stehsel and Waller.[21] Smith[19] observed about a 30% reduction in fracture stress at 4500°F when the strain rate was increased from 8×10^{-5} to 3×10^{-2}/second. This reduction in strength occurs about two to three orders of magnitude of strain rate lower than used in this program and possibly explains the different observation.

The temperature range where the most emphasis was given in this program was from 5000°F to sublimation. Little, if any, data exists on the strength of graphite above about 4500°F, let alone heating rate or time-at-temperature effects. Perhaps the reason for the lack of data is the difficulty encountered in testing at these temperatures. It is imperative that in order to study time dependent heating effects, the duration of the evaluation test (whether it is tensile loading, thermal expansion, or others) must be short compared to the heating time. Otherwise, the effect of heating may be masked by the time involved in the test. The uniaxial high strain rate testing employed in this study has been used and accepted for several years.[1,8,22,23] The heating technique, strain measuring technique, and precision in measuring true temperature are new in this program. Therefore, most of the difficulties previously thought to be barriers to obtaining valid data in this high temperature range have been overcome.

Perhaps the one most difficult task in conducting the tests was measuring temperature. The procedure used is discussed in the Description of Test Technique Section. The key to measuring true temperature was the determination of surface emissivity. This parameter was found to be highly variable to sample preparation technique, atmosphere, temperature, and time. Whether the sample had a highly polished or a dull lathed surface, whether the surrounding gas contained oxygen or argon, and whether the length of time above about 5000° was long or short affected the emissivity. The effect of time appeared to be the most difficult to predict and control. The optical methods that were employed required a relatively long time to obtain data points (about 30 seconds at one temperature). During this time surface changes were so drastic that only average emissivity values could be obtained. In some cases, post heating examination of samples found small bubbles or protrusions on the surface. In others, small holes or pits in the surface were found.

CARBON PHENOLIC (RAD 6300)

Although the objective of this program was to characterize carbon phenolic at all temperatures up to sublimation (∿ 6500°F), emphasis was placed on test temperatures above 2500°F. The reason for this was twofold. First, primary design data was required at temperatures between 4000°F and 6500°F. Second, since carbon phenolic chemically decomposes between temperatures of about 350°F and 1500°F, time-at-temperature and/or heating rate effects in this region would require extremely cautious testing with less confidence in data interpretation. Before uniaxial stress characterization could be conducted at temperatures above 2500°F, a study was made to determine the effect of heating rate through the decomposition temperature range. It was known that phenolic materials could be heated fast enough to make them literally fly apart, or explode. What was unknown was the heating rate required to cause this.

Following the so-called "explosion threshold" tests on carbon phenolic, uniaxial tensile tests were conducted from 2500°F to about 6000°F. Nearly constant heating rates of 10 and 100°F/sec and times-at-temperature from 0 to 100 seconds were investigated.

Explosion Threshold Investigation

The purpose of this investigation was to determine the heating rate where noticeable material degradation was observed. Tests were conducted on carbon phenolic where samples were heated by passing direct current parallel to the fiber layup. Chromel-Alumel thermocouples (0.015 inch diameter) were inserted into the specimen (Figure 23) to measure temperature. Specimens were assembled into the electrical grip/contact assembly with silver paste between the ends and the contact. Initial heating

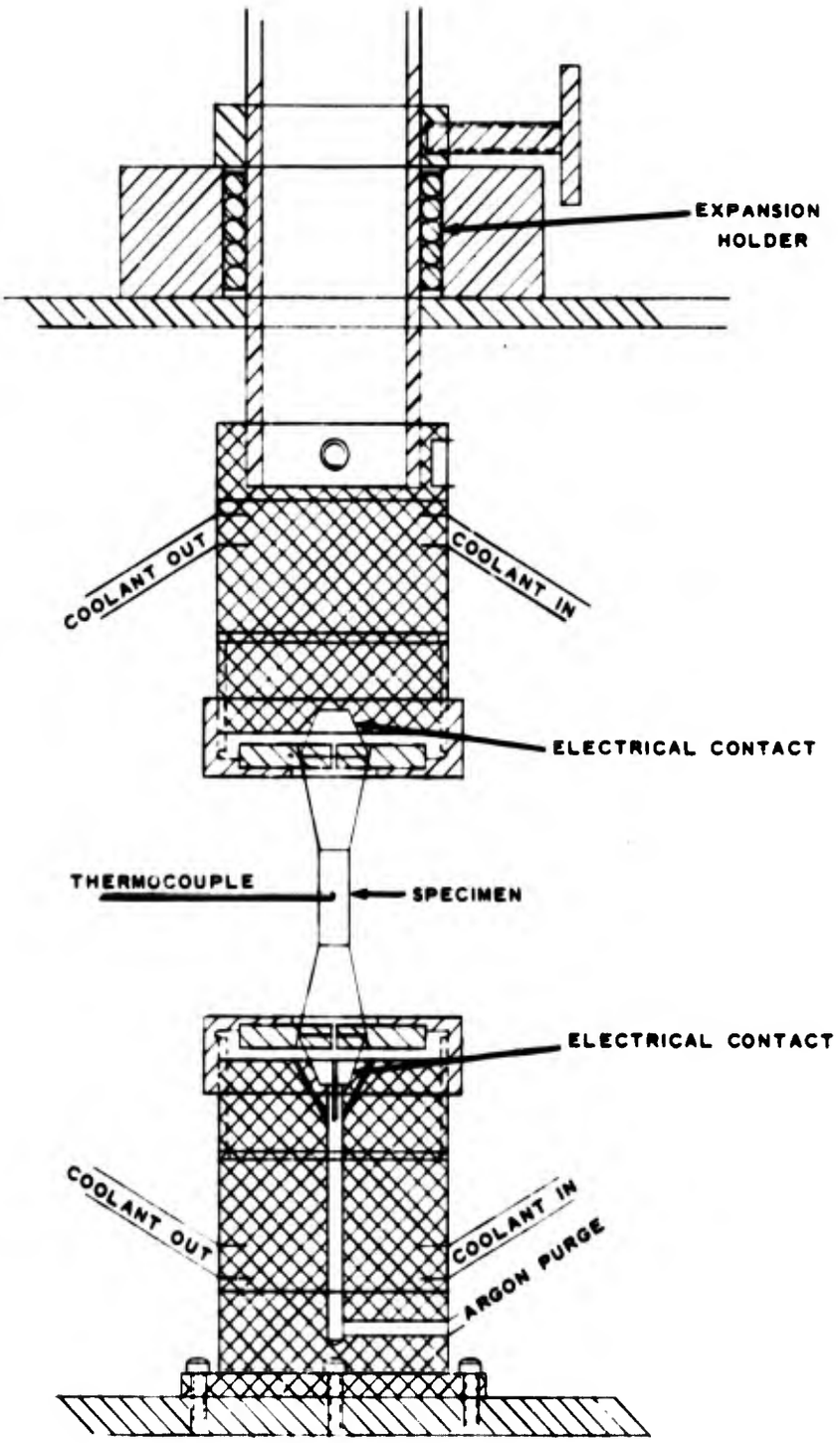

Figure 23 Schematic of Explosion Threshold Experimentation

tests were conducted using a slight argon gas purge around the specimen to minimize surface oxidation. This argon purge was soon found to have no effect on the test results due to the very short heating times, therefore, it was discontinued for the main tests.

Although the primary purpose of this investigation was to determine the heating rates where the material would literally "blow" apart (the explosion threshold), a series of tests was conducted to determine the amount of damage encountered upon heating at rates well below the explosion threshold. As a measure of the extent of material damage, specimen dimensions were measured before and after heating. The specimens were allowed to cool to ambient temperature before taking dimensions after heating.

Table II shows the results of the heating rate tests where the percent dimensional change in two directions (normal and parallel to the fiber layup) is shown along with the average heating rate and maximum temperature attained in each test. A typical temperature-time profile is shown in Figure 24. Attempts were made to heat each specimen at a constant rate. But due to the power supply characteristics and since automatic electronic controls were not employed, heating rates varied by no more than a factor of two during any single test. Figure 25 shows the results in Table II plotted in a semilog scale. Permanent change in two directions and volumetrically is plotted against the log of heating rate. The maximum test temperature was neglected in this plot.

It is seen that a permanent dimensional change of nearly 20 percent was observed normal to the fiber layup while changes generally less than one percent were observed parallel to the layup. Larger scatter was found around 800° to 1500°F/sec.

All of the specimens blew apart at rates greater than about 1500°F/sec. One specimen blew apart around 800°F/sec, a test result unexplained at this time. Photographs of several of the heated specimens are shown in Figure 26.

TABLE II

Effect of Heating Rate on the
Permanent Strain of RAD-6300 Carbon Phenolic

Heating Rate (°F/sec.)	Permanent Strain Normal to Layup (%)	Permanent Strain Parallel to Layup (%)	Maximum Test Temperature (°F)
2.8	1.6	-3.6	1325
32	6.8	0.1	1400
32	6.8	0.1	1400
56	12.9	0.1	1376
183	10.5	-0.4	1437
438	16.8	0.8	1390
811	Fractured	----	1615
856	19.2	0.6	1615
997	18.4	-0.4	1620
1170	12.0	1.6	1437
1281	13.5	0.2	1297
1340	16.0	1.6	1325
1483	19.0	1.0	1632

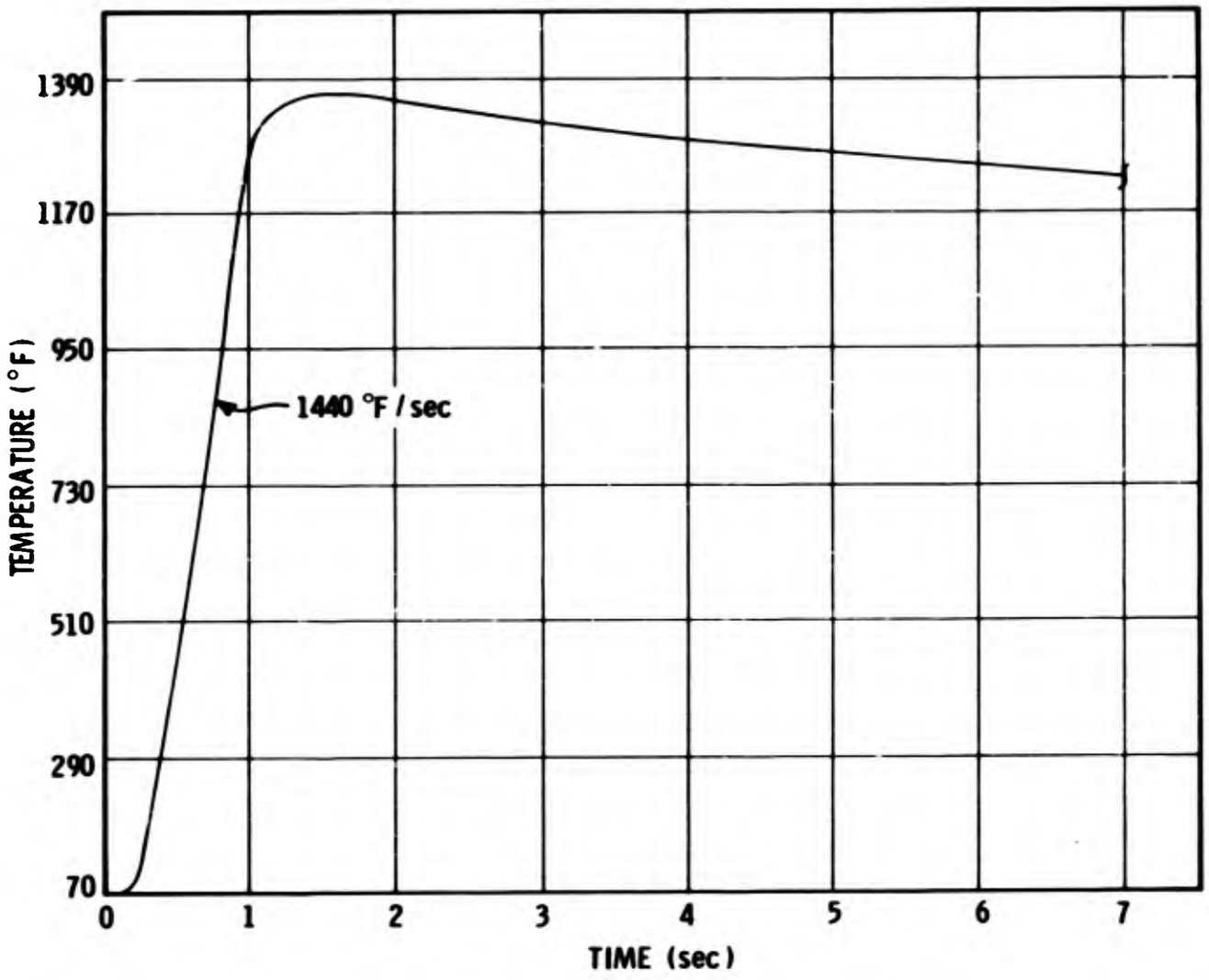

Figure 24 Temperature - Time Curve for Carbon Phenolic

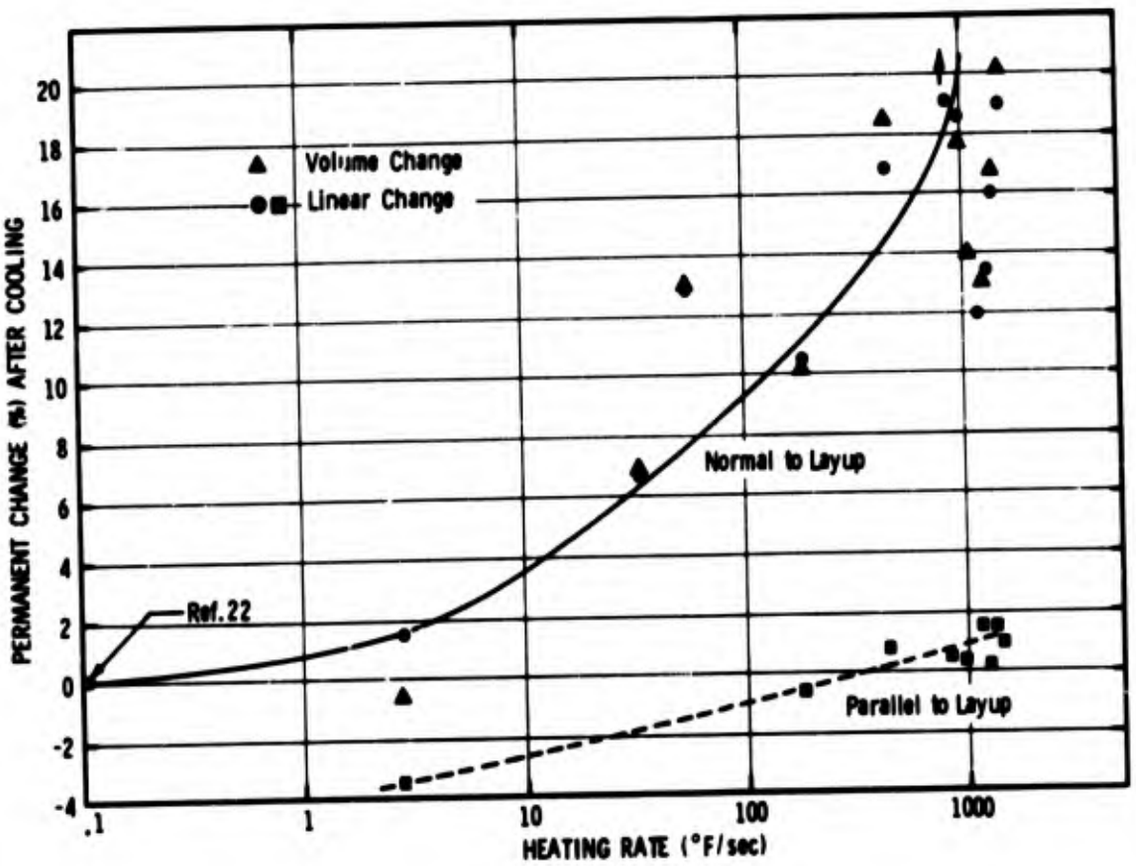

Figure 25 Permanent Changes Versus Heating Rate for Carbon Phenolic

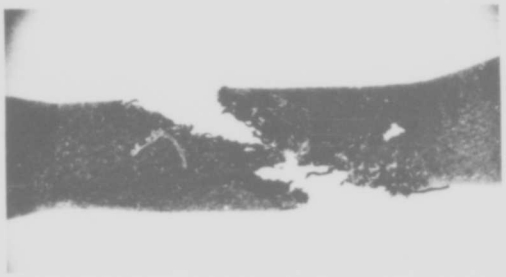

811° F/sec - 1615° F max.

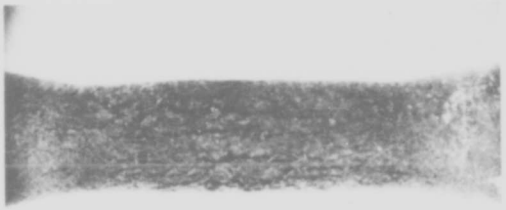

856° F/sec - 1615° F max.
(19.2% expansion)

997° F/sec - 1620° F max.
(18.4% expansion)

Figure 26 Photographs of Rapidly Heated Carbon Phenolic Specimens

Stress-Temperature Results

Figure 27 shows the results of uniaxial tensile tests on carbon phenolic after heating to various temperatures at heating rates up to 100°F/sec. Times-at-temperature of from 0 to 100 seconds were studied. The upper limit of 100°F/sec was selected from the results of the "explosion threshold" investigation. Above this rate, very noticeable macroscopic material degradation was observed due to heating rapidly through the 350°F to 1500°F chemical decomposition range. This temperature range is only approximate, depending on the composite material. Therefore, a low temperature of 2500°F was selected in order to assure nearly all decomposition was completed.

Before any conclusions are drawn from the data in Figure 27, it should be noted that the room temperature tensile strength (with loading parallel to the fiber warp direction) of the RAD 6300 batch used in this program was only about one-half of the previously reported value.[22] The Appendix of this report discusses reasons for this observed difference. In general, material scatter overshadows any heating rate and/or time-at-temperature effects on tensile strength. Data from Ching and Whittier[24] is included in the figure to show the scatter they observed. The heating technique used by Ching and Whittier involved surface heating from a plasma arc. It was shown in a previous report[1] that large thermal stresses are induced in phenolic type ablation materials that are surface heated. The technique used in this study eliminated the large thermal stress gradient. Figure 28 shows the same data as in Figure 27 except data points from the AVCO RADS II[25] studies in the temperature region from 300 to 1000°F are included.

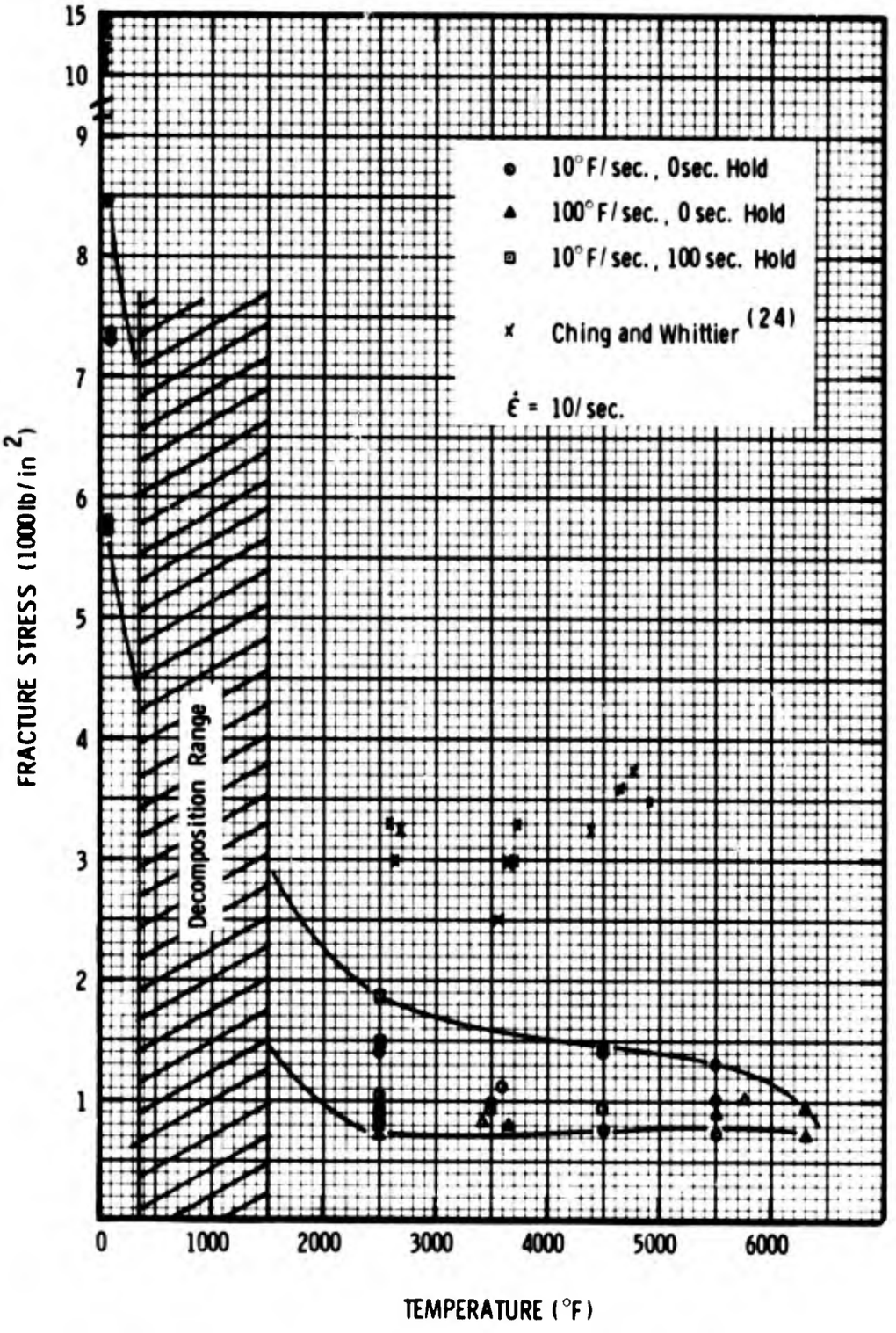

Figure 27 Fracture Stress Versus Temperature for RAD 6300 Carbon Phenolic

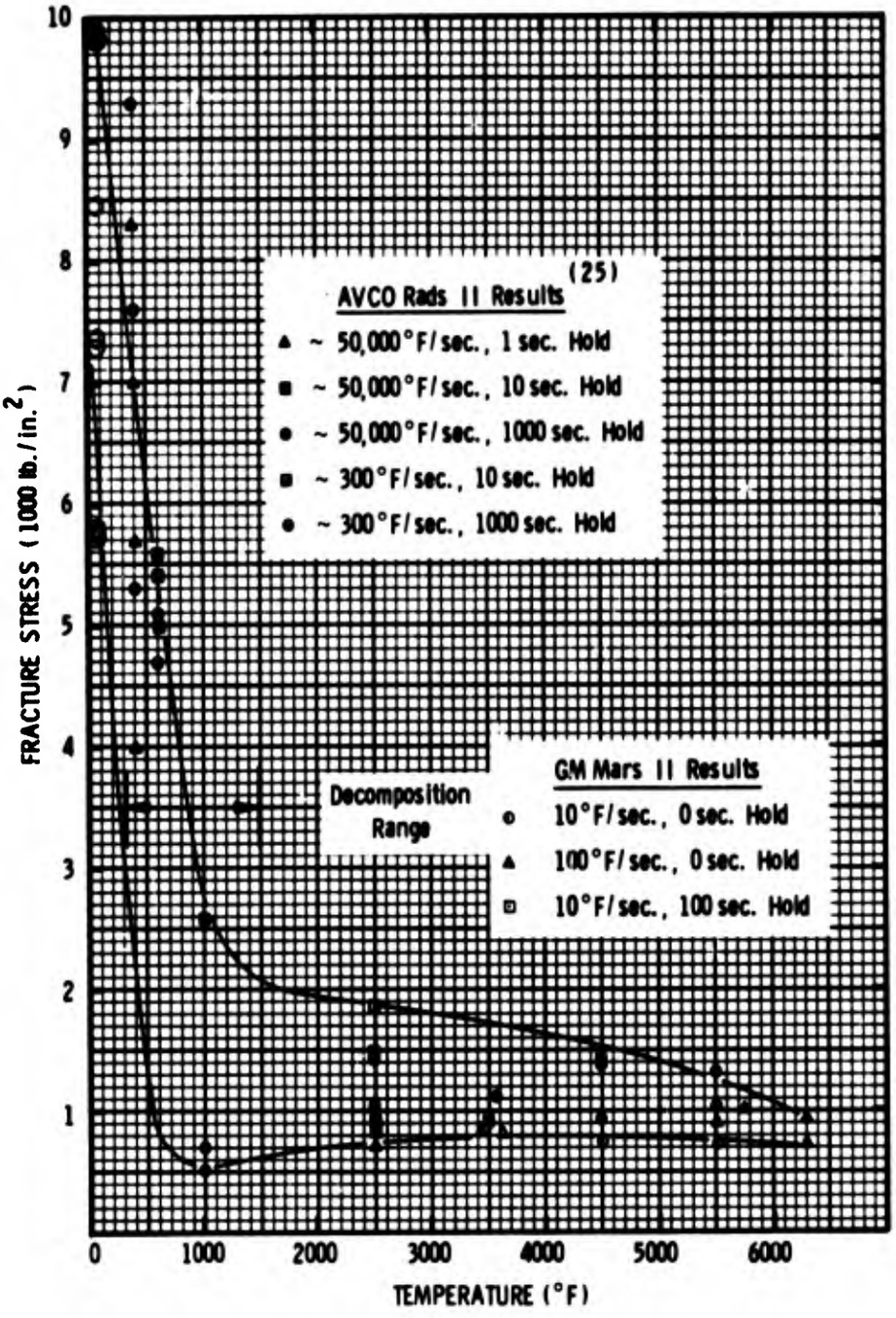

Figure 28 RAD 6300 Carbon Phenolic Fracture Stress - Temperature Relationship

Figure 29 shows stress/strain curves for carbon phenolic under the test conditions where strain was measured. The technique involved using an "effective" gage length along with measuring the lower grip motion. Although fracture stress and modulus are drastically reduced by increasing the test temperature, strain-to-fracture is somewhat temperature sensitive.

The observed effects of heating rate or time-at-temperature on the mechanical behavior of this material is quite complex. The large variation in fracture strength in the decomposition temperature region[25] can probably be described by chemical degradation. Although no obvious time-at-temperature effects on fracture strength are seen, a time/temperature dependence has been observed on modulus (or initial stiffness) for this same material. Landers, et al.[26] described the modulus and strain-to-fracture behavior in terms of a second order chemical reaction above the cure, or glass transition, temperature of the phenolic. Figure 30 shows their uniaxial tensile data, where modulus has been normalized to the room temperature value. It can be seen that at temperatures above about 300°F (near the glass transition) decreasing time-at-temperature reduces the observed modulus. This has been explained as a cross linking chemical strengthening effect, where longer time-at-temperature allows cross linking to increase the modulus.

At 300°F which is below the glass transition and at times too short for any cross linking to occur, decreasing time-at-temperature increases the modulus. This observation is similar to the yield stress increase with increasing heating rates on an aluminum alloy reported by Babcock, et al.[27]

Another interpretation of Landers' data was made by Groves, et al.[28] Noting that Landers reported that mass loss

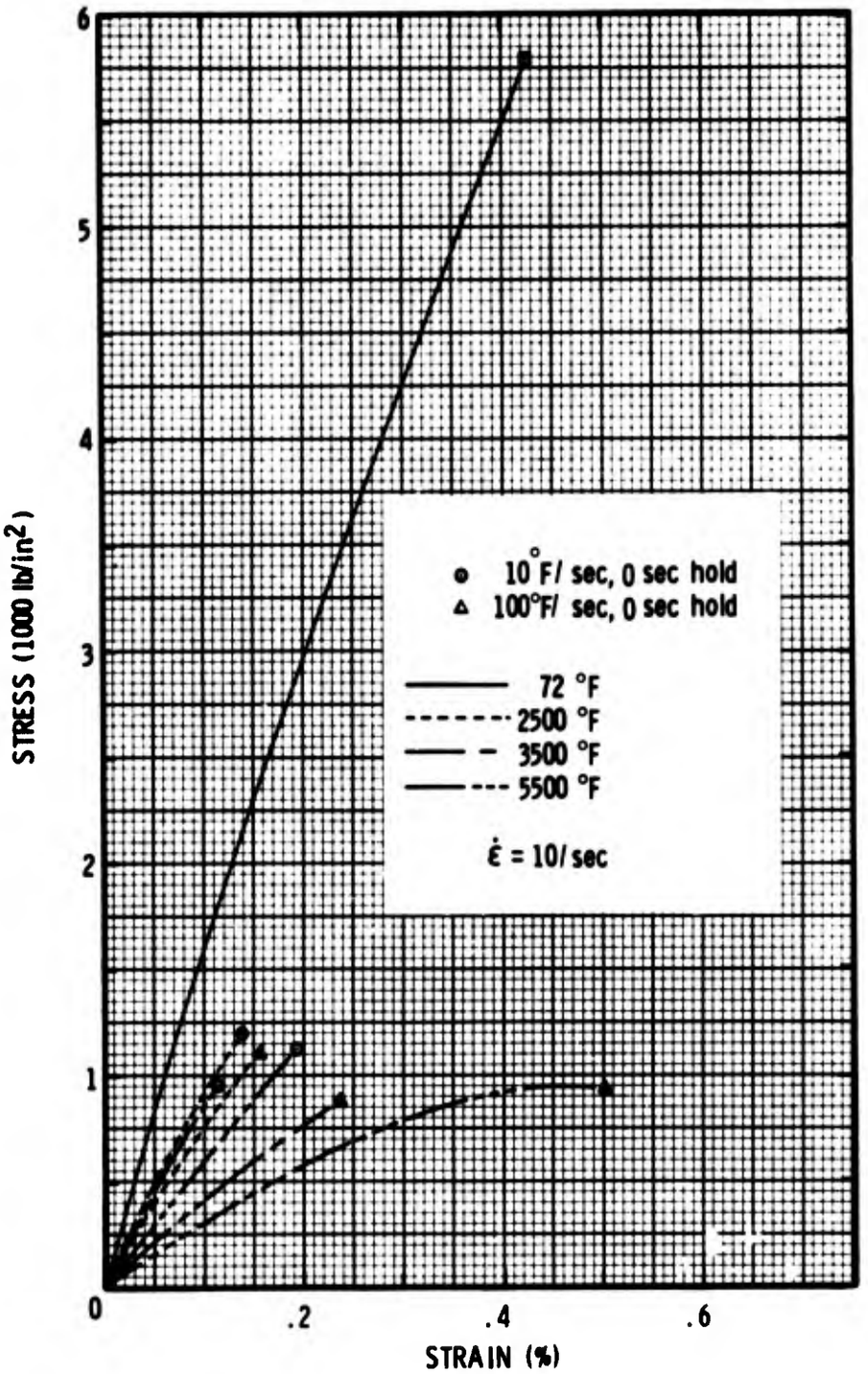

Figure 29 Stress Versus Strain for RAD 6300 Carbon Phenolic

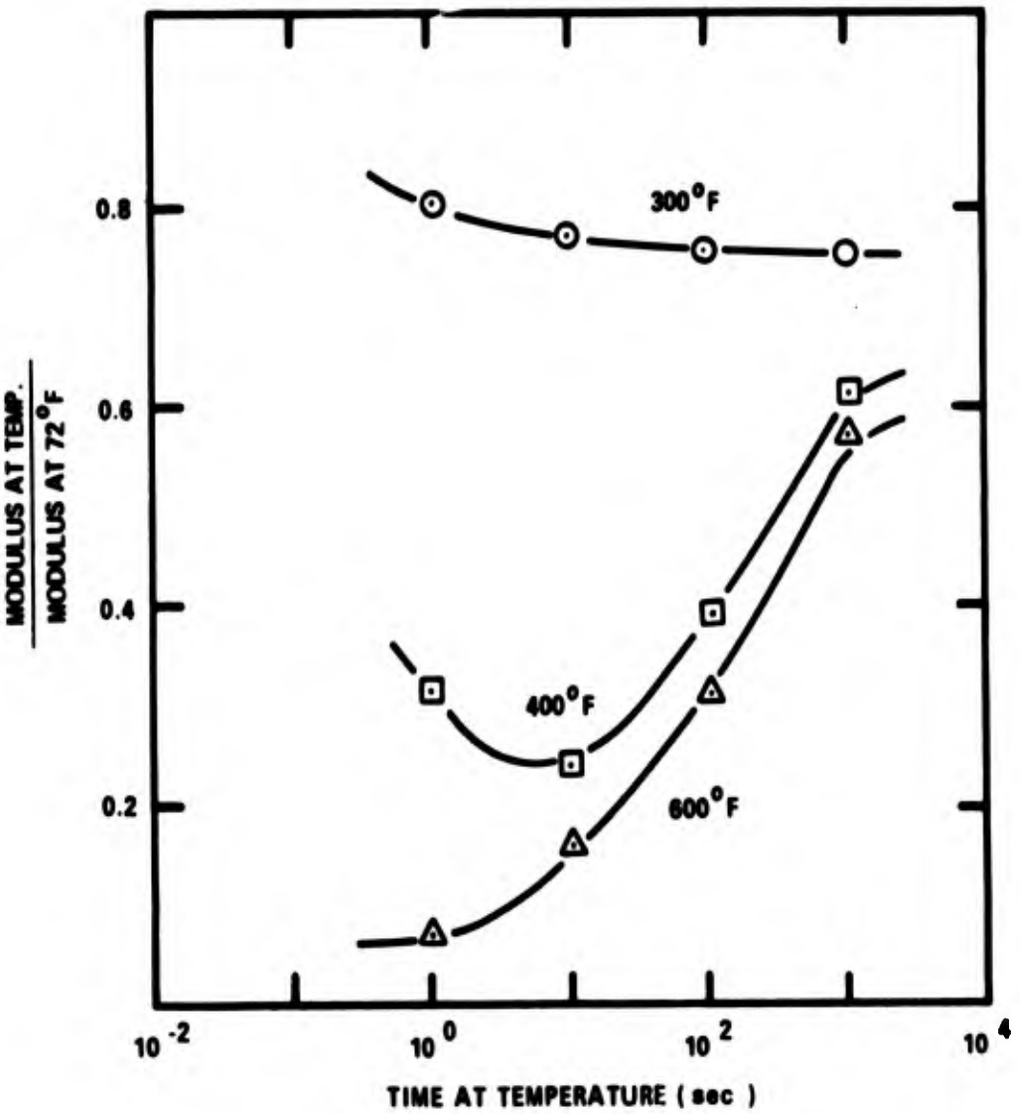

Figure 30 The Effect of Time at Temperature on Initial Modulus for Carbon Phenolic

due to thermal shrinkage of carbon phenolic followed a time to the one-third power dependence upon heating, Groves suggested this phenomenon could be explained in terms of viscoelasticity. According to Schapery,[29] if the molecular structure of a material does not change appreciably during heating

or cooling, or if chemical reaction rates are sufficiently high to maintain chemical equilibrium, such a material can be considered as "thermorheologically simple" and treated in a viscoelastic manner. The differences in thermal coefficients of expansion or contraction in the components of phenolic type composites can cause high internal stresses. The time dependent shrinkage can be explained by the matrix creep compliances where the fibers induce a compressive stress in the matrix upon heating.

The lack of a complete understanding of the mechanical behavior of these materials in the critical decomposition temperature range as well as the very high temperature range is evident from this study. It is obvious from the results presented here that further study on the mechanisms in the deformation behavior of phenolic composites is required.

SECTION III
CONCLUSIONS

1. Testing materials at temperatures up to graphite sublimation (near 6500°F) requires specialized equipment and techniques. Measuring strain and temperature are by far the most difficult and can lead to complications in data interpretation if not properly conducted.

2. ATJ-S graphite exhibits no significant heating rate or time-at-temperature fracture stress effect up to near 5500°F. Above this temperature, time effects appear important.

3. The explosion threshold for RAD 6300 carbon phenolic is near 1000°F/sec heating rate when temperatures in excess of 1000°F are reached.

4. The effect of heating rate or time-at-temperature on RAD 6300 carbon phenolic fracture stress is insignificant when compared to the observed material property scatter.

REFERENCES

1. S. G. Babcock, P. A. Hochstein, and W. F. Dais, "Dynamic Mechanical Properties at Ablative Temperatures--Techniques", Final Report of MARS I, SAMSO TR68-71--Vol. IV, January 1968.

2. H. E. Martens, L. D. Jaffe, and J. E. Jepson, "High-Temperature Tensile-Properties of Graphite", Proceedings of the Third Biennial Carbon Conference, Pergamon Press (1959), p. 529.

3. C. Malmstrom, R. Keen, and L. Green, Jr., "Some Mechanical Properties of Graphite at Elevated Temperatures", J. of App. Physics, Vol. 22, May 1951, p. 593.

4. L. Green, Jr., "High-Temperature Compression Testing of Grahpite", J. of App. Mech., Vol. 20, 1953, p. 289.

5. "A Study of the Effects of Purification on the Tensile Properties of Several Graphite Materials", Final Report to Aerospace Corporation from Southern Research Institute, No. 8608-1759-II, July 1967.

6. R. M. Hale and W. M. Fassel, Jr., "Study of High-Temperature Tensile Properties of ZTA Grade Graphite", Volume 14 of Research and Development on Advanced Graphite Materials, WADD TR61-72, June 1964.

7. W. E. Welsh, Jr., and A. Ching, "A New Technique for Mechanical Strength Testing of Rapidly Charred Ablation Materials", AIAA Journal, Vol. 5, No. 10, October 1967, p. 1882.

8. C. J. Maiden and S. J. Green, "Compression Strain Rate Tests on Six Selected Materials at Strain Rates from 10^{-3} to 10^{4} in./in./sec", J. of App. Mech., Vol. 33, Sept. 1966.

9. J. P. Hirth and G. M. Pound, Condensation and Evaporation Nucleation and Growth Kinetics, MacMillan Co., 1963, N. Y.

10. T. Spalvins, "Energetics in Vacuum Deposition Methods for Depositing Solid Film Lubrications", NASA TMX-52549.

11. P. G. Shewmon, Diffusion in Solids, McGraw Hill, 1963, N. Y.

12. G. S. Anderson, W. N. Mayer, and G. K. Wehner, J. Appl. Phy., 33, p. 2991, (1962).

13. D. J. Healy and M. Lauriente, "Impedance Matching Network for R. F. Sputtering Systems", 13th National Symposium of American Vacuum Society, San Francisco, California, (1966).

14. F. A. Benson and M. W. Bradshaw, "Impedance/Frequency Characteristics of Glow Discharge", Proc. I.E.E., Vol. 113, p. 69, (1966).

15. V. J. D'Amelio and J. A. Roetling, "Extreme Temperature Performance of Graphites", presented at AICHE Materials Conference, Philadelphia, Pa., March 31-April 4, 1968.

16. Reentry Materials Handbook, prepared by Aerospace Corporation for U. S. Air Force, Report No. TOR-1001 (S2855-20)-3, April 1968 (Conf.).

17. S. Mrozowski, "Mechanical Strength, Thermal Expansion and Structure of Cokes and Carbons", Proceedings of the Conferences on Carbon, Pergamon Press, 1953, p. 31.

18. R. J. Diefendorf, "The Effect of Atmosphere on the Strength of Graphite", Proceedings of the Fourth Carbon Conference, Pergamon Press, 1959, p. 489.

19. M. C. Smith, "Effects of Temperature and Strain Rate on Transverse Tensile Properties of H4LM Graphite Tested in Helium and in Vacuum", Carbon, Vol. 1, 1964, p. 147.

20. L. M. Gillin, "Deformation Characteristics of Nuclear Grade Graphites", Journal of Nuclear Materials, Vol. 23, 1967, p. 280.

21. L. Green, Jr., M. L. Stehsel, and C. E. Waller, Mechanical Properties of Engineering Ceramics, Interscience, New York, 1961.

22. S. G. Babcock and R. D. Perkins, "High Strain-Rate Response of Three Heat-Shield Materials at Elevated Temperatures", Vol. II of Material Response Studies (MARS) Final Report, Air Force Contract AF04694-67-C-0033, SAMSO TR68-71, January 1968.

23. S. J. Green, S. G. Babcock, and R. D. Perkins, "Fundamental Material Behavior Study, Vol. I: Response of Several Reentry-Vehicle Materials to Impulsive Loads", Final Report for Air Force Contract AF04-(694)-807, BSD Report TR67-23 (AD822-803L), February 1967.

24. A. Ching and J. S. Whittier, "Summary of High Temperature Mechanical Property Data Obtained with Arc-Heated Specimens", Aerospace Corporation Report TOR-0158 (3240-30)-1, May 1968.

25. J. P. Averell, et al, "Radiation Damage Study-Phase II (RADS II) Final Report - Vol. IX (Simulation Test Techniques)", SAMSO Report TR67-121 - Vol. IX, Prepared by AVCO Missile Systems Division, November 1967 (SRD).

26. L. L. Landers, Jr., J. Atkinson, and C. C. Theberge, "Effects of Time at Temperature on the Mechanical Properties of a Fabric Reinforced Phenolic Heat Shield Material", Proceedings of AIAA/ASME 10th. Structures, Structural Dynamics, and Materials Conference, April, 1969, p. 183.

27. S. G. Babcock, S. J. Green, and D. B. Norvey, "Effect of High Heating Rate on the Yield of 6061-T6 Aluminum", to be published.

28. R. N. Groves, Jr., J. L. Wheeler, and R. A. Schapery, "A Final Report on Heating Rate and Time at Temperature Effects for Phenolic Reentry Heat Shield Materials", report to General Motors Manufacturing Development by Midwest Applied Science Corporation, October, 1968.

29. R. A. Schapery, "Stress Analysis of Viscoelastic Composite Materials", J. of Composite Materials, Vol. 1, 1967, p. 228.

30. R. D. Perkins, et al, "Multiaxial Loading Behavior of Four Materials Including ATJ-S Graphite and RAD 6300 Carbon Phenolic", Final Report on Material Response Studies (MARS II) under Air Force Contract F04701-68-C-0161, March 1970.

APPENDIX

DISCUSSION OF RAD 6300 CARBON PHENOLIC MECHANICAL PROPERTIES

Several reports[22,23,30] in the past two years have been published on the mechanical strain rate properties of RAD 6300 carbon phenolic. These reports indicate that a large variation in properties, such as initial modulus and fracture strength, can be expected in this material. An attempt is made in this Appendix to correlate and discuss these observed variations in order to give greater confidence to the user of the data.

Two suppliers were used to fabricate the RAD 6300 carbon phenolic test materials reported in References 22, 23 and 30 namely, AVCO* and HAVEG**. The AVCO material was fabricated in compression molded panels approximately 0.625" X 6" X 6" and 3.5" X 12" X 12" in size. The HAVEG material used in this report and Reference 30 was fabricated in 3.75" X 12" X 12" compression molded panels and bias tape wrapped tubular cylinders, approximately 3" O.D. X 6" long X 0.25" wall and 3" O.D. X 6" long X 0.375" wall. The same components were called for in the specification and the end result indicated densities close to 1.40 gm/cm^3 for all the material.

Figure A-1 shows the uniaxial compressive behavior of RAD 6300 carbon phenolic when loaded parallel to the fiber layup (edge compression). These results, from HAVEG 3 3/4" block material, encompass strain rates from 10^{-3} to 2 X 10^3/second and temperature of 72° to 800°F. Figure A-2 is a cross plot from Figure A-1

---

* AVCO Corporation, AVCO Missile Systems Division, Wilmington, Mass.

** HAVEG Industries Inc., Reinhold Aerospace Division, Santa Fe Springs, California.

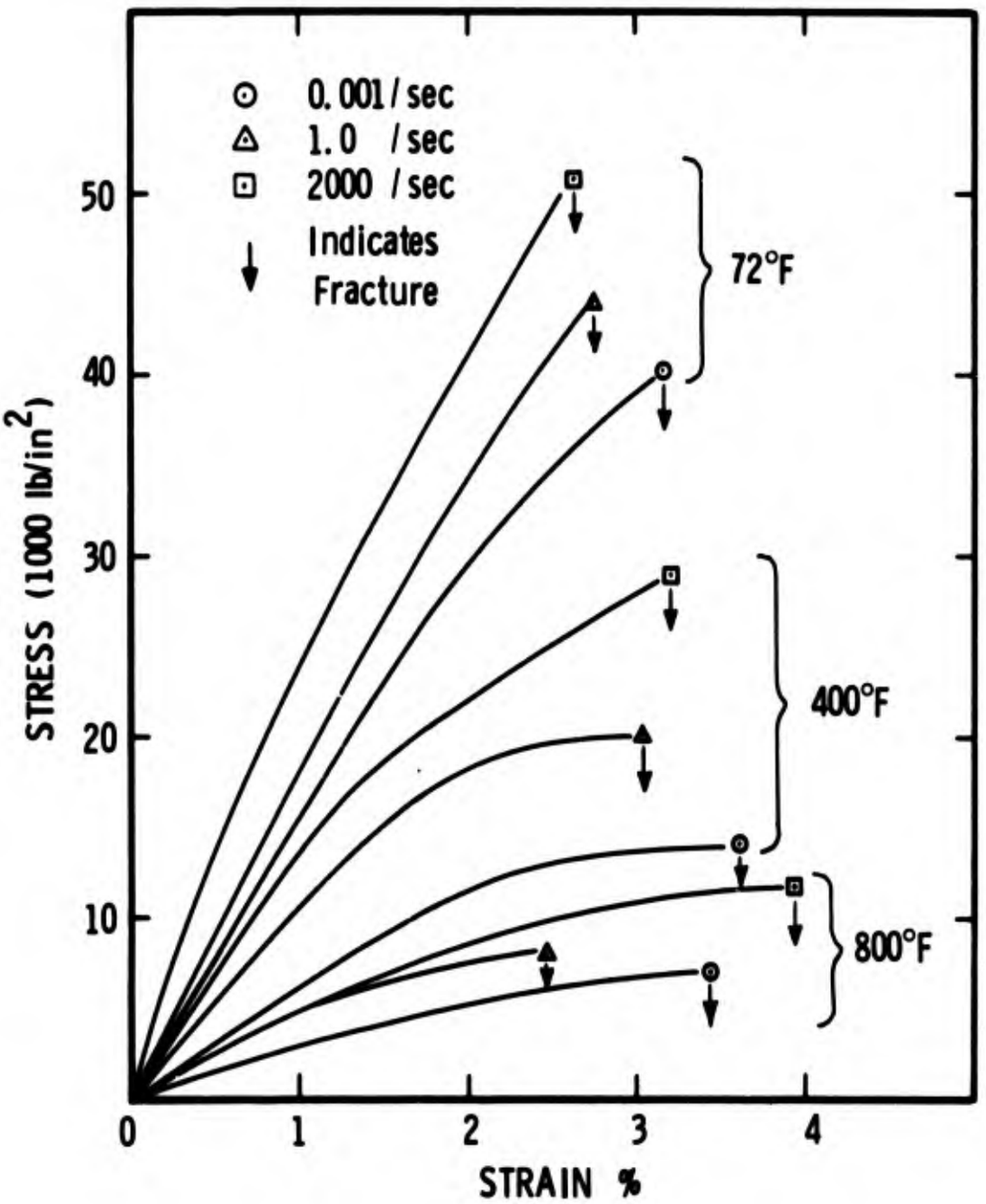

Figure A-1 Compression Test Results on RAD 6300 Carbon Phenolic - Loaded Parallel to Layup

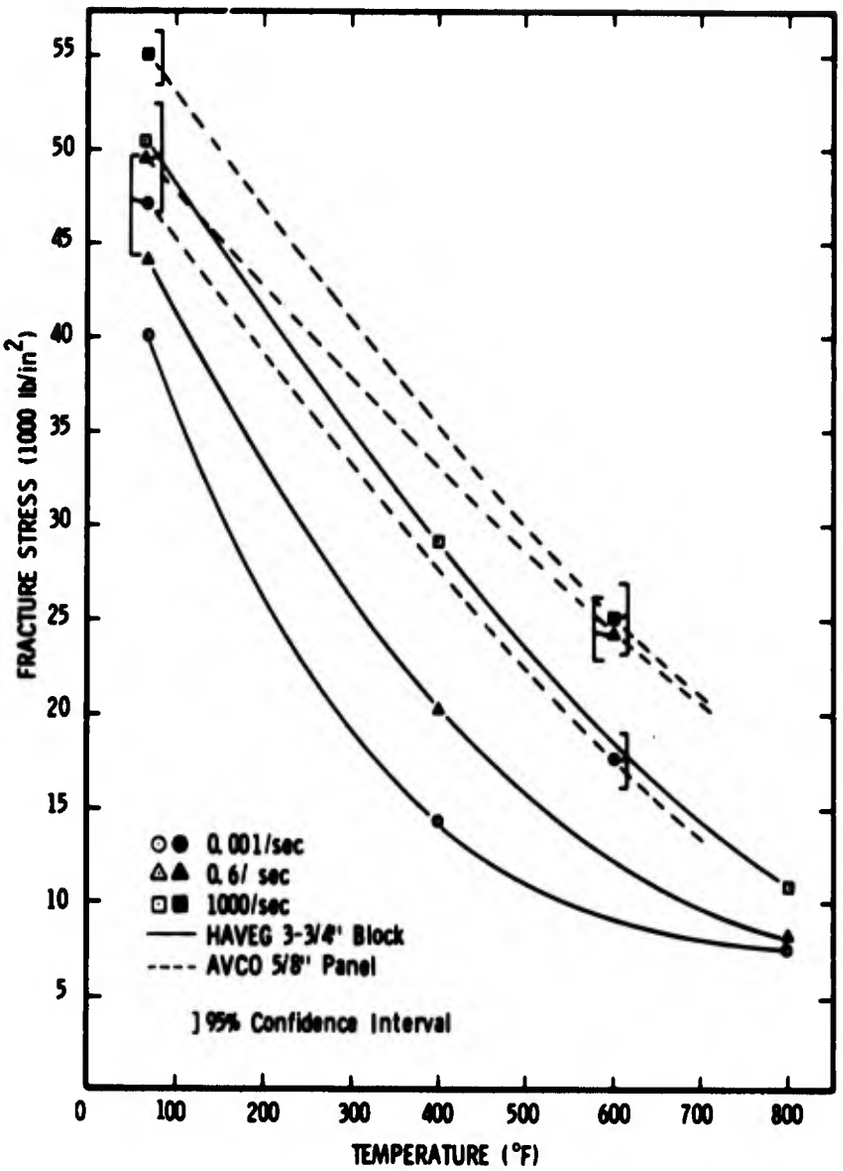

Figure A-2 Compressive Fracture Stress Versus Temperature for RAD 6300 Carbon Phenolic - Loaded Parallel to Layup

where fracture stress is plotted against test temperature. Included in this figure are results from AVCO 5/8" block material. There are obvious differences between the two lots of material, nearly 50% difference in some cases, and completely outside the 95% confidence intervals shown in the figure. Figure A-3 is a stress-strain plot of the room temperature results presented in Figure A-2 with an added comparison from the HAVEG 3/8" wall tubular cylinder material.

Perhaps an even more illustrative example of differences between so-called RAD 6300 carbon phenolic is shown in Figure A-4. Four different lots of material are shown where tensile stress-strain results parallel to the fiber layup at two strain rates are plotted. Here it is clear that the size of the molded panel drastically effects the modulus and tensile fracture stress. The smaller panels (or fewer plys) give higher moduli and tensile strengths.

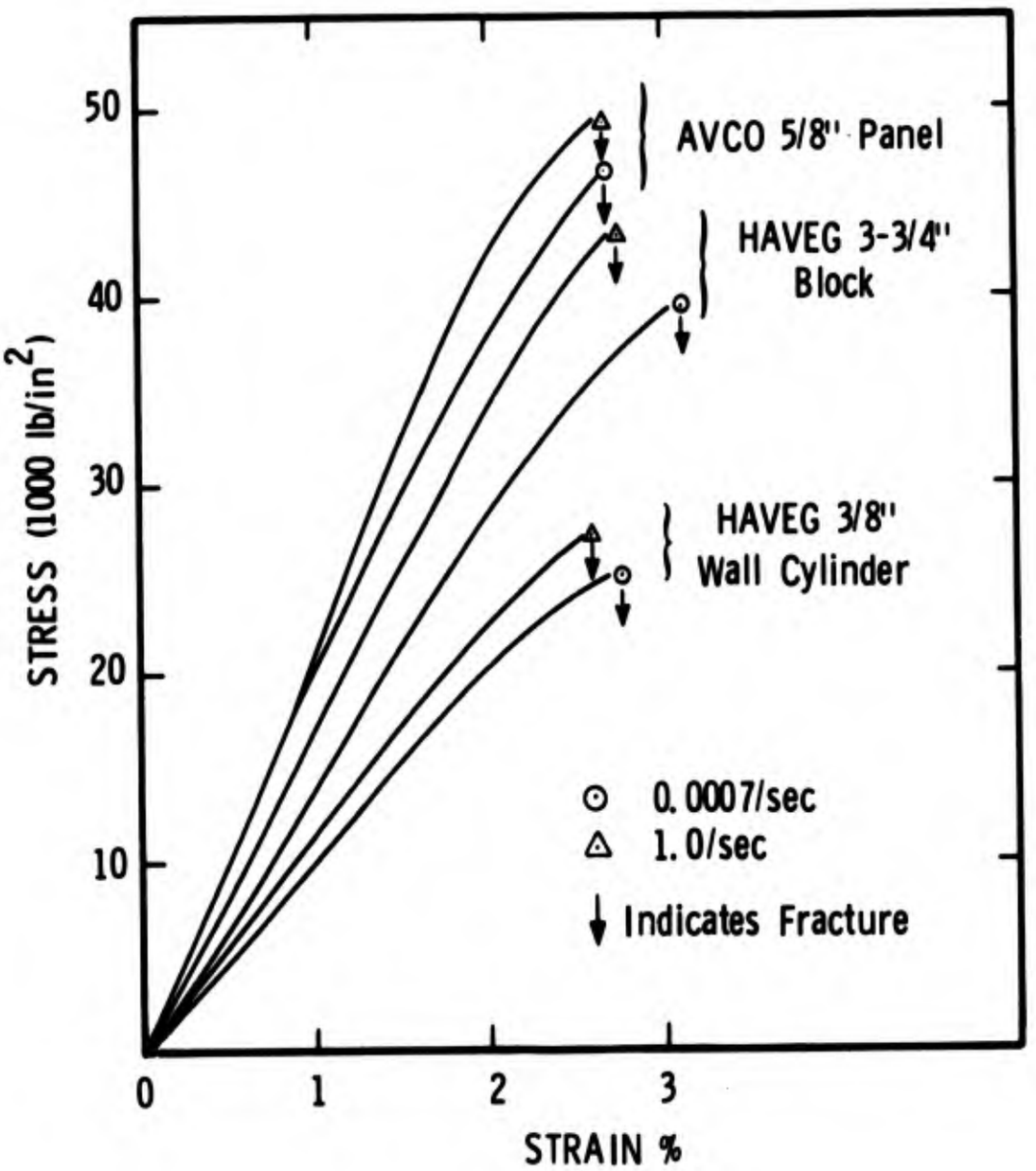

Figure A-3 Compressive Stress Versus Strain Room Temperature Results for RAD 6300 - Loaded Parallel to Layup

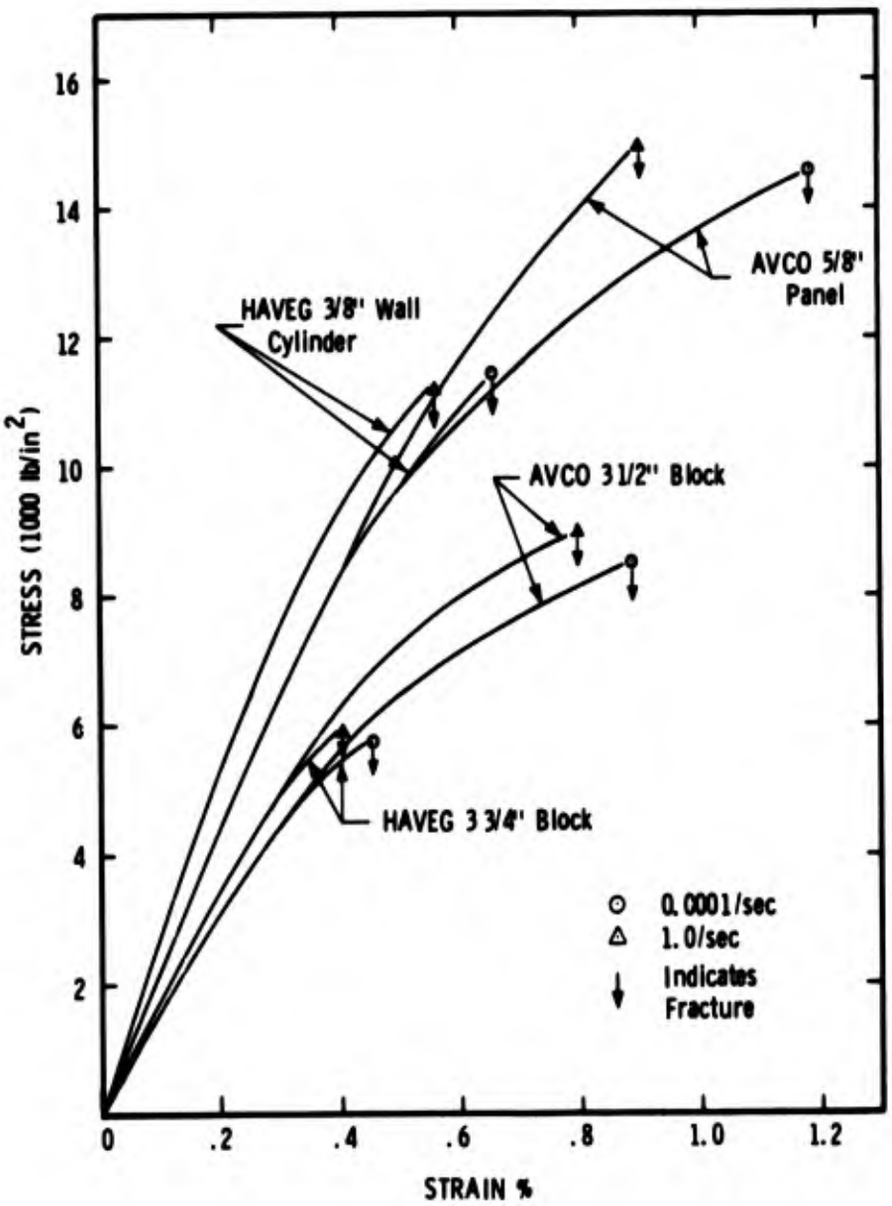

Figure A-4 Tensile Test Results on RAD 6300 Carbon Phenolic - Loaded Parallel to Layup

UNCLASSIFIED

Security Classification

DOCUMENT CONTROL DATA - R & D

(Security classification of title, body of abstract and indexing annotation must be entered when the overall report is classified)

1. ORIGINATING ACTIVITY *(Corporate author)*
Manufacturing Development
General Motors Corporation, General Motors Technical Center, Warren, Michigan 48090

2a. REPORT SECURITY CLASSIFICATION
UNCLASSIFIED

2b. GROUP

3. REPORT TITLE
FINAL REPORT MATERIALS RESPONSE STUDY (MARS II) VOL. II: HIGH HEATING RATE RESPONSE OF TWO MATERIALS FROM 72 TO 6000°F

4. DESCRIPTIVE NOTES *(Type of report and inclusive dates)*
Final Report (In Two Volumes)

5. AUTHOR(S) *(First name, middle initial, last name)*
S. G. Babcock, P. A. Hochstein, L. J. Jacobs

6. REPORT DATE	7a. TOTAL NO. OF PAGES	7b. NO. OF REFS
1970, March	78	30

8a. CONTRACT OR GRANT NO.	9a. ORIGINATOR'S REPORT NUMBER(S)
F04701-68-C-0161	
b. PROJECT NO.	MSL-69-48 Vol. II
c.	9b. OTHER REPORT NO(S) *(Any other numbers that may be assigned this report)*
d.	SAMSO TR-69-393, Vol. II

10. DISTRIBUTION STATEMENT
This document may be further distributed by any holder only with specific prior approval of Space and Missile Systems Organization (SMYSE), Norton Air Force Base, California 92409

11. SUPPLEMENTARY NOTES
The distribution of this report is limited because it contains technology requiring strict approval of all disclosures by SAMSO.

12. SPONSORING MILITARY ACTIVITY
Space and Missile Systems Organization
Deputy for Ballistic Missile Re-entry Sys.
Air Force Systems Command
Norton Air Force Base, California

13. ABSTRACT

This report describes the results of a study to characterize two graphitic materials, graphite (ATJ-S) and carbon phenolic (RAD 6300), in uniaxial stress after undergoing heating to temperature near 6500°F. Heating rates up to 1000°F/second and strain rates up to 10/second were investigated. Test results as well as a complete description of the experimental techniques developed in this program are discussed. Techniques include measuring strain using a laser extensometer, coating thin films on graphite using r.f. sputtering, and determining true test temperature.

DD FORM 1 NOV 65 1473

UNCLASSIFIED

Security Classification

14. KEY WORDS	LINK A		LINK B		LINK C	
	ROLE	WT	ROLE	WT	ROLE	WT
ATJ-S graphite						
RAD 6300 carbon phenolic						
High Temperature						
High Heating Rate						
Strain Rate						
Sublimation						